

UNIVERSITY OF OKLAHOMA

GRADUATE COLLEGE

DIURNAL CHANGES IN SURFACE URBAN HEAT ISLANDS AND THEIR
RELATIONSHIPS WITH URBAN LAND COVER

A THESIS

SUBMITTED TO THE GRADUATE FACULTY

in partial fulfillment of the requirements for the

Degree of

MASTER of SCIENCE

By

Nikhil Raj Poudyal

Norman, Oklahoma

2024

DIURNAL CHANGES IN SURFACE URBAN HEAT ISLANDS AND THEIR
RELATIONSHIPS WITH URBAN LAND COVER

A THESIS APPROVED FOR THE
DEPARTMENT OF GEOGRAPHY AND ENVIRONMENTAL
SUSTAINABILITY

BY THE COMMITTEE CONSISTING OF

Dr. Michael C. Wimberly, Chair

Dr. Chengbin Deng

Dr. Nishan Bhattarai

© Copyright by Nikhil Raj Poudyal 2024

All Rights Reserved.

ABSTRACT

Urbanization, a prominent phenomenon since the industrial revolution, has led to significant changes in land use and land cover (LULC), resulting in the Urban Heat Island (UHI) effect. This effect, characterized by higher temperatures in urban areas compared to their rural surroundings, is influenced by the use of heat-absorbing materials, human activities, and urban geometry. The resulting high temperature affects urban residents with implications for public health, greater energy consumption, and change in local climatology. Understanding the spatial variations in land surface temperature (LST) and the thermal effects of heterogeneous urban forms is essential for developing mitigation strategies to enhance the urban thermal environment.

A modern method introduced in the past decade in urban climatology is the concept of the local climate zone (LCZ). This approach disaggregates the heterogeneity in urban settings and classifies surfaces into various built and natural land cover types, which in turn helps to interpret the patterns of LST in the local surrounding area. Previous studies have shown that different urban structures, such as residential areas, commercial zones, and industrial regions, exhibit varying surface temperature patterns. In developing countries, urban planning often results in heterogeneous urban landscapes with mixed land uses, further complicating the UHI dynamics. This study investigates the relationship between various LCZs and their LSTs in the cities of Ahmedabad and Surat in the state of Gujarat in India. The LCZ map used in this study was created from a fusion of two data sets: 1) a freely available 100m global LCZ map, and 2) a 30m land use land cover (LULC) map developed using Landsat-8 data.

A few studies have explored the diurnal variations of LST over urban areas, mainly due to the revisit cycles of polar orbiting satellite (e.g., Landsat Series, Terra, Aqua). However, in this study, we leverage LST data from The National Aeronautics and Space Administration's (NASA) latest Ecosystem Spaceborne Thermal Radiometer Experiment on Space Station (ECOSTRESS) that provides LST at 70m resolution at different diurnal periods. Then we studied how LST changes within different LCZs at various times of day to understand the thermal effects of urban landscapes.

The results reveal distinct seasonal and diurnal variations in LST. During winter, Surat exhibited consistently higher temperatures than Ahmedabad, with differences averaging around 5°C. In summer, temperatures rise significantly in both cities, peaking at 40°C in Surat and 45°C in

Ahmedabad. Several LST hotspots were identified, particularly in industrial areas and densely built-up zones. For instance, an international airport in Ahmedabad showed temperatures up to 52°C on summer afternoons, significantly higher than the surrounding areas.

Distinct thermal patterns were observed across LCZs during different diurnal periods. Compact midrise areas were the hottest, while open lowrise areas were cooler during both seasons and across all diurnal cycles in both cities. Large lowrise areas were typically hotter than compact lowrise areas in the mornings and afternoons. However, large lowrise areas cooled faster, making them cooler than compact lowrise areas during the evenings and nights. In both cities, compact midrise and compact lowrise areas exhibited the highest temperatures in the evening and nighttime.

The study also analyzed the diurnal variations in LST gradients from the center to the edges of the city, revealing that during summer mornings, there was a negative correlation between LST and distance from the city center. This correlation weakened in the afternoon but strengthened again in the evenings and nights, particularly in Ahmedabad. Both cities showed stronger negative correlations in the evenings and nights, indicating a pronounced UHI effect while in the afternoon there was no correlation as the solar radiation was heating the surface uniformly.

This study emphasizes the value of using the new ECOSTRESS LST products for analyzing diurnal thermal variations with fine spatial resolution. These findings offer an understanding of the impact of various urban structures on local climate aiding city planners and developers in implementing informed heat mitigation strategies. However, the use of ECOSTRESS data comes with limitations, such as the day and night LST data not being from the same day, causing inaccuracies and uncertainties. Additionally, cloud cover can result in missing grid cells, and variations in viewing angles due to the ISS's orbit can affect the accuracy and consistency of LST measurements.

ACKNOWLEDGEMENTS

I would like to express my sincere gratitude to my supervisor and committee chair, Prof. Dr. Michael C. Wimberly, for his invaluable advice, guidance, supervision, discussions, and critiques throughout the journey of this research. I would also like to thank and acknowledge the genuine support and feedback from Assoc. Prof. Dr. Chengbin Deng and Asst. Prof. Dr. Nishan Bhattarai, and for agreeing to serve as committee members. I also extend my thanks and appreciation to the faculty, staff, and members of my graduate program in the Department of Geography and Environmental Sustainability (DGES).

I am grateful to DGES for providing me with various graduate funding opportunities during my program and supporting me in every viable way. I also express my heartfelt thanks to my friend, Asst. Prof. Dr. Dan Wanyama, for teaching and assisting me with various R-related topics and GIS-related issues; it was truly an amazing learning experience.

My gratitude extends to all the members of the EcoGRAPH Research Group for creating a lovely working environment and for sharing knowledge and experiences.

Finally, I would like to thank my beloved wife, my two amazing kids, and my wonderful parents for their constant support and encouragement, making my life a joyful journey. Thank you, God, for sending all these helpful hands to me and making me more capable and stronger so I can help and support others equally.

TABLE OF CONTENTS

ABSTRACT.....	iv
ACKNOWLEDGEMENTS.....	vi
List of Figures.....	ix
List of Tables.....	xi
1. INTRODUCTION.....	1
1.1. Background and Rationale.....	1
1.2. Research Problem and Significance of the Study.....	4
1.3. Research Objectives.....	7
2. LITERATURE REVIEW.....	8
2.1. Urban heat islands and basic energy exchange concept.....	8
2.2. Relationship between surface and air temperatures.....	9
2.3. Relationship between LST and Land cover/Land use.....	11
2.4. Local Climate Zones (LCZs) and urban structure types.....	12
3. STUDY AREA.....	16
3.1. Ahmedabad City.....	17
3.2. Surat City.....	18
4. DATA AND METHODOLOGY.....	20
4.1. General Framework.....	20
4.2. LULC map production and Fusion with LCZ map.....	21
4.3. ECOSTRESS data and processing.....	25
4.4. Data Analysis.....	28
4.4.1. Monthly LST trend analysis.....	28
4.4.2. Descriptive analysis of LST spatial patterns.....	29
4.4.3. Quantitative analysis of relationships between LST and LCZs.....	29
4.4.4. Quantitative analysis of LST gradient from city core to edge.....	29
5. RESULTS.....	31
5.1. Average monthly LST.....	31
5.2. Visual interpretation of LST hotspots and urban structures.....	32
5.3. Diurnal LST relationship with LCZ classes.....	36
5.4. LST gradient analysis.....	39

6. DISCUSSION AND CONCLUSION	43
7. LIMITATIONS AND RECOMMENDATIONS.....	47
APPENDICES	49
Appendix 1. Earth observation (EO) input features for LCZ (Demuzere et al., 2021).....	49
Appendix 2. Tables representing ECOSTRESS data download and processing statistics.....	50
Numbers representing data available from downloads to various processing steps.....	50
Segregation of data availability for each season and time of day	50
Monthly data available after visually selecting and geo-referencing	51
Appendix 3. Ahmedabad LULC map accuracy and confusion matrix	51
Appendix 4. Surat LULC map accuracy and confusion matrix	52
Appendix 5. Ahmedabad Landsat-8 scenes used for LULC classification in Google Earth Engine.....	52
Appendix 6. Surat Landsat-8 scenes used for LULC classification in Google earth Engine. ..	53
List of References	54

List of Figures

Figure 2.1: Energy Balance diagram for urban area, adapted from Zhou (D. Zhou et al. 2019). Red arrow represents energy input while blue represents energy departing from urban system....	9
Figure 2.2: Differences between surface and air temperature in an urban settlement	10
Figure 2.3: Local climate zones classification scheme and 17 standard classes with brief definition (Stewart and Oke in 2009). © Copyright 2012 AMS.....	13
Figure 3.1: Location map of the study area, Ahmedabad and Surat, zoom imagery taken from Esri, Maxar, World imagery	16
Figure 3.2: Average minimum and maximum temperature in Ahmedabad and Surat cities, © Copyright 2022 weather-and-climate.com.....	18
Figure 3.3: Average precipitation in Ahmedabad and Surat city,.....	19
Figure 4.1: General framework of the research	20
Figure 4.2: LULC remapped schema to fuse with LCZ urban built classes.....	23
Figure 4.3: Classes obtained after fusion (remapping), and classes under analysis are marked with star.....	23
Figure 4.4: LULC remapped with LCZ map to produce a fused map for Ahmedabad city	24
Figure 4.5: Flow chart representing the data processing using R on ECOSTRESS data to extract cloud free and of better quality. Orange box section was done manually using ArcGIS Pro.....	26
Figure 4.6: Screen shot of ArcGIS Pro showing a misaligned ECOSTRESS data along with manually selected control points to guide the alignment process, while referencing the satellite image on the background	27
Figure 4.7: Ahmedabad city boundary ‘a’ and Surat city boundary ‘b’ shown as blue polygons overlaid over Nighttime light data from VIIRS and Google Map	28
Figure 4.8: Displaying 1000 random points along with the centroid over Ahmedabad. Satellite image as background (left), Euclidean distance as background (right)	30
Figure 5.1: Monthly average LST trend of two cities, Ahmedabad and Surat	31
Figure 5.2: Ahmedabad city, Land cover map (top left), Summer (March-June) average LST from ECOSTRESS (top right). 4 zoomed images of hotspot zone a, b, c, and d taken from Esri, Maxar, World imagery (bottom 4)	33

Figure 5.3: Surat city, Land cover map (top left), Summer afternoon (March-June) average LST from ECOSTRESS (top right). 4 zoomed images of hotspot zone a, b, c, d taken from Esri, Maxar, World imagery (bottom 4)	34
Figure 5.4: Semi-transparent LST image over highly vegetated residence and its urban surrounding (a). Very-high resolution imagery of the corresponding region (b).....	36
Figure 5.5: Group box plot of LST comparing each city (Ahmedabad and Surat) for different LCZs at different times of the day in summer. Center line in the box represent median, edges of the box represent the first quartile (Q1) and third quartile (Q3), and whiskers represent the range within 1.5 times the interquartile range (IQR) from Q1 and Q3.	37
Figure 5.6: Group box plot of LST comparing each city (Ahmedabad and Surat) for different LCZs at different times of the day in winter. Center line in the box represent median, edges of the box represent the first quartile (Q1) and third quartile (Q3), and whiskers represent the range within 1.5 times the interquartile range (IQR) from Q1 and Q3.	38
Figure 5.7: Ahmedabad LST gradient from the center of city towards rural areas during different times of the day and seasons.	41
Figure 5.8: Surat LST gradient from the center of city towards rural areas during different times of the day and seasons.....	42

List of Tables

Table 4.1: List of Input features fed to random forest classifier.	21
Table 4.2: Details of the downloaded ECOSTRESS data using AppEEARS portal.	25

1. INTRODUCTION

This chapter introduces the background and justification for ongoing research in the field of Urban Heat Island (UHI) phenomenon and its relationship with various land surface types that form localized climate zones. Here we identify the research problem and describe research objectives.

1.1. Background and Rationale

After the industrial revolution in the late 18th century, and by the mid-19th century, urbanization accelerated in Europe and North America. The trend continued into the 20th century, especially after World War II, when urbanization started spreading to other parts of the world, including Asia, Latin America and Africa (United Nations., 2019). A UN report (United Nations., 2016) estimates that currently, 50% of the world population lives in cities and it is projected to be 66% by 2050. The urban population growth rate averaged approximately 2.5% per year globally between 1950 and 2000. Some regions, particularly in developing countries, have experienced even higher rates. For example, the urban population in Africa grew at an average annual rate of 3.5% from 1950 to 2000 and continues to grow rapidly. Between 1980 and 2010, China's urban population grew at an average annual rate of approximately 3.9%. India has also experienced an increase in its urban population. Between 1950 and 2000, India's urban population growth rate averaged around 3.1% per year (United Nations., 2019).

Migration from rural areas to cities is driven by several key factors. Economic opportunities in urban areas, such as higher wages and diverse job prospects, attract individuals seeking better livelihoods. Urban centers typically offer improved access to education, healthcare, and social services, enhancing quality of life. Additionally, cities provide better infrastructure and amenities, including transportation, housing, and entertainment (United Nations., 2016).

Even though urbanization may be associated with growth in the human development index¹ (UN-Habitat, 2011), it comes with its own challenges and complexities that may impact the environment and communities living in it. With more human population concentration there

¹ The Human Development Index (HDI) is a composite statistic used by the United Nations to measure and rank countries' levels of social and economic development.

is always an increase in infrastructure buildup leading to alteration in land use and land cover (LULC), where natural land surfaces are converted to impervious surfaces altering the physical properties of the surface (Argüeso et al., 2015). This urbanization and population growth, when combined with climate change impact, is a recipe to put cities' social and ecological environments at substantial risk. For example, rapid urbanization is responsible for the degradation of ecosystems, increase in heat waves, irregular precipitation, urban flash floods, water scarcity, and degraded air quality (Malik et al., 2020).

One significant impact of urbanization is an increase in surface temperature. According to the IPCC (Intergovernmental Panel on Climate Change) report, global surface temperatures will continue rising throughout the 21st century (*AR5 Climate Change 2014*, n.d.). This change will result in more heatwaves that increase potential risk to public health. Heatwaves can lead to heat-related illnesses such as heat exhaustion and heatstroke, and they can worsen preexisting health conditions, particularly in vulnerable populations like the elderly and children. Heatwaves also lead to an increase in energy consumption patterns by driving up the demand for air conditioning and cooling systems, resulting in higher electricity use. This surge in energy demand puts additional stress on power grids and can lead to higher greenhouse gas emissions if the energy is sourced from fossil fuels. Thus, as global temperatures rise, heatwaves become more common and severe, creating a feedback loop that further accelerates climate change (Clinton & Gong, 2013; L. Lu et al., 2020).

In the study of various temperature patterns and heatwaves in cities, an important & widespread phenomenon is the urban heat island (UHI). This effect can be defined as anomalies in temperatures between urban areas and their rural surroundings, where temperatures within the urban areas are higher than in the surrounding rural and natural landscapes (Oke, 1982; Voogt & Oke, 2003).

Several physical processes contribute to the UHI effect. Absorption and retention of heat from heat-absorbing materials such as concrete and asphalt over urban surfaces are some of the major factors contributing to the UHI effect. These materials retain heat absorbed from solar radiation during the day and slowly release it at night, causing urban spaces to be warmer than their rural counterparts (Rizwan et al., 2008). Additionally, human activities in urban areas, such as transportation, industrial processes, and energy consumption, release heat directly into

the environment. This anthropogenic heat adds to the overall temperature of the urban area. Further, urban surfaces and their physical features are often characterized by low albedo, which is the measure of how much sunlight is reflected by a surface (D. Zhou et al., 2019). Darker surfaces, like asphalt and buildings, have low albedo and absorb more solar radiation, contributing to higher temperatures. Additionally, there is little vegetation to cool these surfaces. Although vegetation has a low albedo, it cools surfaces by dissipating energy through the process of evapotranspiration (Zölch et al., 2016). Also, tall buildings and other tall urban structures disrupt the natural flow of air leading to lower ventilation and trapping hot air within the urban boundaries (Yow, 2007).

Oke (Oke, T.R. et al., 1976, 1982) classified UHI into two categories: air and surface UHI. Air is considered the canopy urban heat island (CUHI), and the land surface is considered the surface urban heat island (SUHI). The canopy here represents the layer of air a few meters above ground (usually about 2m) therefore, CUHI relates to temperature differences in the canopy layer of urban areas compared to the canopy layer of rural surroundings. In contrast, SUHI refers to the temperature difference of the land surface temperature or skin temperature, between urban areas and the surrounding rural areas. CUHI is measured using in-situ temperature sensors typically mounted on a fixed platform or sometimes a moving vehicle that gives a reading of air temperature, whereas SUHI is measured by calculating the difference in radiant temperature captured by thermal remote sensors. The radiant temperature is sensitive to surface moisture and land surface conditions, exhibiting a high level of variation even across small spatial and temporal scales (Kustas & Anderson, 2009). Although the in-situ data can provide accurate and high-temporal surface temperature information, these methods of observation are limited in numbers, making them inefficient for mapping UHI across a large area (Firozjaei et al., 2018; Han et al., 2020). Hence, it is necessary to utilize remote sensing data, which are spatially continuous and measured over large areas, to examine the detailed spatiotemporal patterns of the SUHI (Weng et al., 2019; D. Zhou et al., 2019). This study we will exclusively focus on thermal remote sensing data and will not incorporate in-situ air temperature data.

Remote sensing data are also extensively used for LULC mapping/change which allows the study of urban infrastructure, population growth, and other factors that have significant effects

on UHI characteristics. For instance, in a study by Bokaie (Bokaie et al., 2016), Landsat Thematic Mapper was employed to map the UHI of Tehran for the year 2010. They examined the connection between the LULC map and the Normalized Difference Vegetation Index (NDVI). Their findings revealed an association between LST and LULC classes. Additionally, they observed a negative correlation between LST and NDVI. If details about the urban structure types can be discriminated into various urban subclasses, such as densely built residential areas, sparse residential areas, industrial zones, roads, vegetation, and water bodies, it can enhance our understanding of UHIs and their effects. Hence, a better understanding of urban structure types, including their physical and functional characteristics, can help identify the factors contributing to variation in surface temperatures which in turn provides valuable insights into the UHI phenomenon.

1.2. Research Problem and Significance of the Study

Stewart and Oke (Stewart & Oke, 2012) introduced the novel concept called Local Climate Zone (LCZ) which serves several purposes in urban climatology and urban planning. For example, LCZs are used for urban climate classifications that help researchers and planners understand the unique climate conditions. LCZs also serve as input parameters for urban microclimate models, which simulate the complex interactions between urban form, land use, and meteorological conditions. In this study, we utilize LCZs to examine the temperature patterns within the urban areas by categorizing the surface form into various LCZs. Previous studies have mostly explored the sub-categorically classified urban structure types and their effect on LST distribution across cities from developed countries (X. Zhou et al., 2020; Středová et al., 2021; Wei & Sobrino, 2024). Unlike cities in developed countries, developing countries' urban characteristics are quite different in terms of urban planning. For instance, urban planning in developing countries is usually heterogeneous with mixtures of ununiformly distributed commercial, residential, and industrial areas within the city boundary. This pattern results from rapid urbanization and loosely regulated land use policies, creating diverse and mixed-use urban environments (Sun et al., 2016). Therefore, it is equally significant to study the influence of such composition of land surface patterns in developing countries that impact local LST patterns.

SUHI has come into focus only in the last two to three decades with the use of satellite remote sensing and our knowledge of this phenomenon is still evolving. However, there are some limitations imposed by currently available data sources. The polar-orbiting satellite data on SUHI is limited by its repeat cycle, while geostationary satellites cannot offer a high spatial resolution. Therefore, this tradeoff restricts satellite observations, making it challenging to observe the diurnal UHI cycle at a finer spatial scale. Landsat is a common source of LST data for UHI observation and is a sun-synchronous satellite with observations at around 10:30 am in the morning at a native resolution of 100m and a repeat cycle of 16 days. Another common source of remotely sensed LST data is MODIS, with its Terra and Aqua observations providing daily data at 10:30 a.m. and 10:30 p.m., and 1:30 a.m. and 1:30 p.m., respectively at 1km resolution with revisit time of 1-2 days. On the other hand, Geostationary Operational Environmental Satellites (GOES) provide thermal data at a spatial resolution of 2km with observations every 15 minutes. Numerous UHI studies have utilized single all-clear sky images from Landsat or coarse-resolution data from MODIS (Peres et al., 2018; Ferreira & Duarte, 2019; Gohain et al., 2021; Z. Zhao et al., 2021). However, these approaches often fall short in distinguishing the fine details of various surface types due to their limited spatial resolution (Hulley et al., 2019). Landsat's imagery, while clearer, captures less temporal variability, and MODIS data, despite frequent coverage, lacks the necessary granularity. Consequently, these methods are insufficient for accurately mapping the heterogeneous urban surfaces that contribute to UHI effects. On the other hand, GOES satellite's temporal resolution is 15 minutes, but its relatively low spatial resolution of 2 km limits the number of local-scale studies on SUHI (Chang et al., 2022).

Studies conducted using Landsat overlook the diurnal pattern while those using MODIS fails to provide the required granular details of the UHI, resulting in a significant gap in understanding the fluctuations in UHI characteristics throughout the day, including morning, afternoon, evening, and night. It is essential to investigate these variations across all urban LCZ to recognize the underlying causes and effects of temperature fluctuations associated with different urban surface types. To better understand the dynamics of urban heat and its implications for urban environments, it is essential to recognize that SUHI effects exhibit distinct patterns during the day and night. Therefore, we need to analyze how LCZ effects vary at various times of the day to capture these variations comprehensively.

To the best of our knowledge, no detailed study has been conducted over the study area that focuses on LCZs in Ahmedabad and Surat. While there are numerous papers on UHI in Indian cities including Ahmedabad and Surat (Gohain et al., 2021; Siddiqui et al., 2021; Shahfahad et al., 2021, 2022), our research is novel in two key aspects: (1) analyzing urban classes based on LCZs scheme, and (2) leveraging ECOSTRESS data to obtain high-resolution LST measurements across four diurnal cycle over the LCZs.

Here, we utilize the capabilities of a relatively new experimental sensor, ECOSTRESS, which was launched in 2018 and is stationed onboard the International Space Station (ISS) (discussed in Chapter 4, Data and Method). What sets ECOSTRESS apart is its distinctive orbital path, enabling it to revisit locations every three days. Moreover, its orbit permits image capture at any time of day or night, acquiring images across various time periods and allowing coverage of different temporal conditions. Another advantage of this dataset is its native resolution of 70 meters which is better than any freely available LST dataset (Hook et al., 2020; Hulley et al., 2022).

Given the preceding information, studies correlating urban surface type and LST in the context of developing countries with such a moderate resolution of 70m are still scarce. This study aims to enhance past studies and gain enhanced information about specific factors that contribute to higher surface temperature with spatiotemporal variability of UHI. The results from this study will contribute to the knowledge of LCZ in the study area, contributing towards obtaining practical knowledge on the cause and effect of increasing LST due to urbanization. Finally, this study is expected to offer valuable insights into land planning and urban design policies aimed at mitigating the UHI effect within the urban contexts of developing countries.

1.3. Research Objectives

The primary objective of this study is to analyze the correlation between LST and urban structures using the LCZ concept. To achieve this objective and ensure accurate measurement and interpretation of results, the study aims to address the following four sub-objectives.

- To map LCZs in the study area by fusing a global LCZ dataset with local land cover information.
- Assess the characteristics of urban hot spots across various locations within the urban environment.
- Analyze the relationship between LST and LCZs across four diurnal periods (morning, afternoon, evening, and night) and two seasons (winter and summer).
- Explore the change in LST from the city center to the edge across the four diurnal periods and two seasons.

2. LITERATURE REVIEW

Understanding the dynamics of urban LST and their associations with land cover surface class is essential for addressing the challenges of the UHI phenomenon. Numerous studies have explored the relationship between urbanization processes and the resulting changes in LST. Bokaie (Bokaie et al., 2016) mentions that urban LST patterns are significantly influenced by the type of land cover surface materials. A heterogeneous mixture of land cover materials and a complex biophysical process triggers a chained feedback loop that contributes to the UHI pattern (Clinton & Gong, 2013; L. Lu et al., 2020). This literature review aims to explore these dynamics, examining the several factors influencing urban heat patterns and the role of different urban surface classes.

2.1. Urban heat islands and basic energy exchange concept

UHIs are the result of replacing natural land surfaces with human-caused urban surfaces that result in differences in surface energy balance and eventually cause increases in urban temperature. According to Zhou (D. Zhou et al., 2019) urban surface energy balance can be represented as.

$$Q_I + Q_{L\downarrow} + Q_F = Q_R + Q_{L\uparrow} + Q_E + Q_H + Q_S \text{ (Graphical representation in Figure 2.1)}$$

Where Q_I = incident solar radiation, $Q_{L\downarrow}$ = incoming longwave radiation, Q_F = anthropogenic heat releases, Q_R = reflected solar radiation, $Q_{L\uparrow}$ = outgoing longwave radiation, Q_E = latent heat, Q_H = sensible heat, Q_S = heat storage. In the case of thermal remote sensing, satellites measure the $Q_{L\uparrow}$ to later convert it to surface temperature (Voogt & Oke, 2003). The increase in $Q_{L\uparrow}$ which represents the increase in UHI is an increase in longwave radiation influenced by various energy fluxes and differs between daytime and nighttime conditions. During the day, urban surfaces absorb solar radiation and release it as heat, contributing to elevated temperatures. At night, urban areas retain more heat due to the thermal properties of building materials and the reduced cooling effects of vegetation, resulting in higher nighttime surface temperatures compared to rural areas (Deilami et al., 2018). Therefore, understanding the dynamics of energy fluxes within urban environments is crucial for understanding the diurnal variations in the UHI effect and its implications for urban climate and heat management strategies.

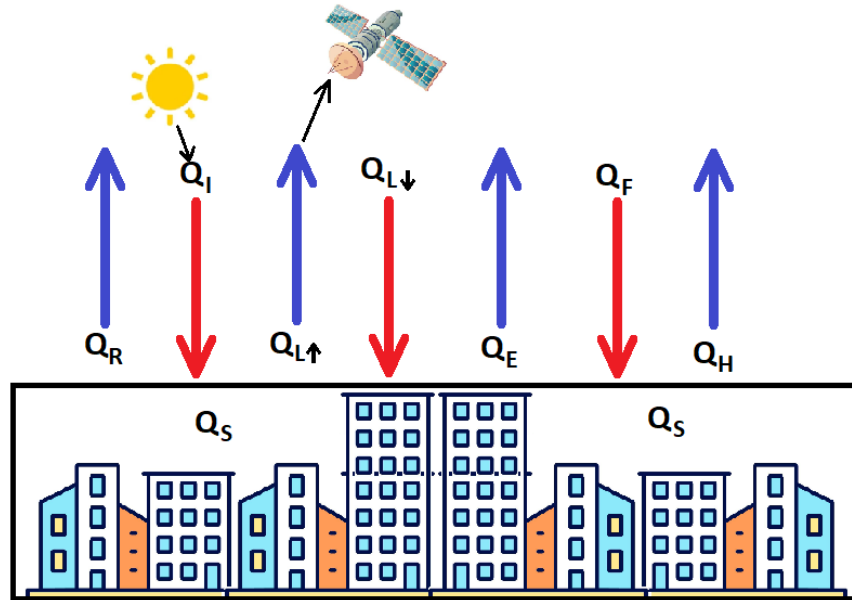


Figure 2.1: Energy Balance diagram for urban area, adapted from Zhou (D. Zhou et al. 2019). Red arrow represents energy input while blue represents energy departing from urban system

2.2. Relationship between surface and air temperatures

As mentioned by Nichol, (Nichol, 1994) LSTs are considered to represent a proxy indicator of the CUHI as there are often high correlations between LSTs and air temperature, especially during nighttime. However, due to the mixing of air in the above-ground atmosphere, the relation between them is not constantly linear. As illustrated in Figure 2.2 (US EPA, 2014), there is less spatial variation in air temperature compared to LST during the day, whereas a closer relationship between the two variables can be observed at nighttime.

During the day, LST varies significantly across different urban and rural areas. Figure 2.2 shows that surface temperatures are highest in downtown urban areas and industrial zones, where impervious surfaces like concrete and asphalt absorb and retain heat. In contrast, areas with water bodies, parks, and suburban regions exhibit lower surface temperatures due to higher albedo and cooling effects from vegetation and water. Air temperature, however, shows less spatial variation during the day. This is because air, unlike surfaces, mixes, and redistributes heat more evenly. As a result, while urban areas still experience higher air temperatures due to localized heating, the difference between urban and rural air temperatures is not as distinct as the difference in surface temperatures (US EPA, 2014).

At night, the relationship between LST and air temperature becomes more aligned. The heat stored in urban materials during the day is gradually released, keeping higher temperatures for both surface and air temperatures over urban areas (W. Zhang et al., 2011). This nighttime heat release contributes significantly to the UHI effect. Figure 2.2 indicates that both surface and air temperatures in urban areas remain higher than in rural areas at night, reflecting the heat retention properties of urban materials (US EPA, 2014).

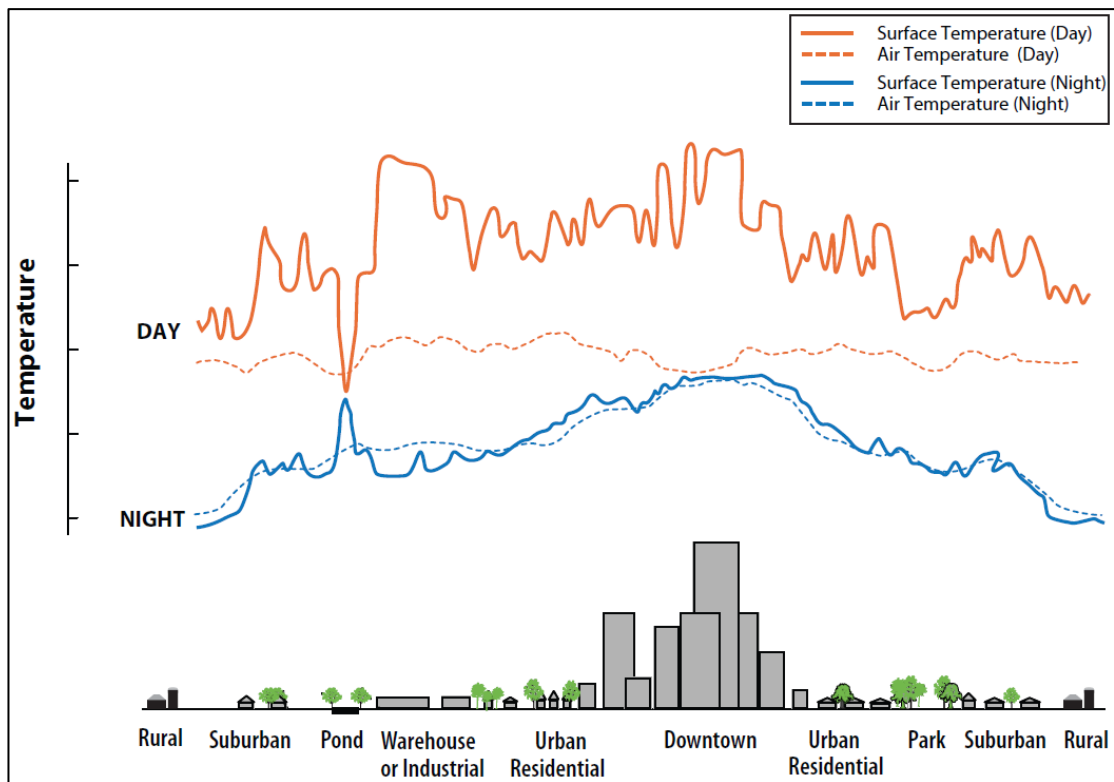


Figure 2.2: Differences between surface and air temperature in an urban settlement (US EPA 2014)

2.3. Relationship between LST and Land cover/Land use

After the introduction of remote sensing technology and the proliferation of freely available LST data, much research has been conducted to investigate SUHI patterns and their spatial variations and correlations with land surface type (Voogt & Oke, 2003). Guha (Guha et al., 2018) used Landsat-8 data for mapping UHI in two cities in Italy where they found that about 75% of UHI was concentrated within bare land and urban build-up areas. Chen (Y.-C. Chen et al., 2017), examined the diurnal variation of LST over the Taipei city in Taiwan using MODIS and SPOT multispectral images and found a linear increase in temperature with an increase in urbanization. They calculated urbanization using cell-average NDVIs & cell-based urbanization index with SPOT multispectral image. In another study by Peres (Peres et al., 2018), they used a 30 year time series of SUHI data to compare it with LULC maps over Rio de Janeiro. They concluded that an increase of 2 degrees Celsius was associated with rapid urban expansion. A study conducted by Gohain (Gohain et al., 2021) in Pune, India suggested that the LST varied spatially over the city and underwent seasonal changes while buildup of urbanized land cover had higher LST. In another study in Beijing by Feng (Feng & Myint, 2016), they analyzed the effect on LST due to neighboring land cover patterns around the building areas, which were categorized into low-rise, mid-rise, and high-rise buildings. They found that the composition of land cover features exerts a more pronounced influence on the LST of low-rise buildings compared to that of mid-rise and high-rise buildings. Additionally, the LST of low-rise buildings was significantly correlated with the types of neighboring land cover, particularly the presence of vegetation and pavement. The presence of nearby greenery led to lower LST, while extensive pavement coverage increased it. Similarly, Zhou (W. Zhou et al., 2011), studying the Gwynns Falls watershed in Baltimore, found that areas with a higher percentage of built-up structures tend to have higher LST, whereas regions with a higher percentage of natural vegetation mitigated the UHI effect by reducing the local temperature.

Zhang (X. Zhang et al., 2009) investigated the influence of vegetation patch size on urban LST and found that larger areas with abundant green patches lowered the surface temperature. Well-vegetated areas can mitigate the SUHI effect through several mechanisms. Although they typically exhibit a low albedo, meaning they absorb a significant portion of incoming solar radiation, they still reduce heat absorption by the surface through processes like

evapotranspiration and shading. Evapotranspiration cools the air as water evaporates from the leaves (Q_E , latent heat loss in Figure 2.1), and shading reduces the amount of solar radiation that reaches the ground and built surfaces, thereby lowering overall temperatures (Zölch et al., 2016).

2.4. Local Climate Zones (LCZs) and urban structure types

As discussed in Section 1.2, LCZs were defined and developed by Stewart and Oke (Stewart & Oke, 2012) as a framework to serve multiple purposes in urban climatology and urban planning. In this study, we utilize the LCZ classification to categorize urban areas based on their physical characteristics and thermal properties. The LCZ system divides cities into various homogeneous urban zones, providing a localized land cover classification for urban climate modeling (Danylo et al., 2016). Specifically, LCZs classify urban areas into 17 distinct LCZs, each with unique characteristics, as illustrated and defined in Figure 2.3. There are two types of zones; the first one is called land use type which is basically the built-up area. They are sub divided into 10 different zones. The second one is classified as land cover type and contains 7 different zones as shown in Figure 2.3.

Bechtel (Bechtel et al., 2015) focused on the global mapping of LCZs, providing a standardized method for characterizing urban structures based on their intrinsic physical and thermal properties, rather than local LCLU classifications such as built-up areas or natural vegetation. This distinction is important because LCZs offer a more detailed representation of urban environments, which is crucial for climate studies. Unlike traditional LCLU classifications that primarily categorize land based on surface cover types (e.g., residential, commercial, forest, water bodies), LCZs classify urban areas into specific zones based on structural characteristics, such as building height, density, surface cover, and materials. This approach results in 17 distinct LCZs (Figure 2.3), each with unique climate-relevant properties, allowing for a more precise analysis of urban climate dynamics.

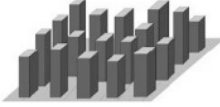
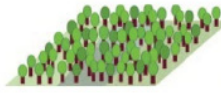
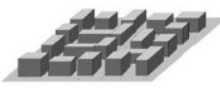
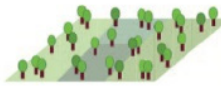
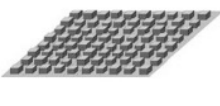
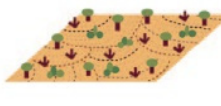



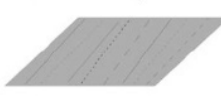


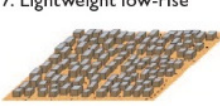
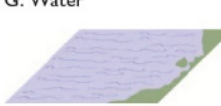



Built types	Definition	Land cover types	Definition
 <p>1. Compact high-rise</p>	Dense mix of tall buildings to tens of stories. Few or no trees. Land cover mostly paved. Concrete, steel, stone, and glass construction materials.	 <p>A. Dense trees</p>	Heavily wooded landscape of deciduous and/or evergreen trees. Land cover mostly pervious (low plants). Zone function is natural forest, tree cultivation, or urban park.
 <p>2. Compact midrise</p>	Dense mix of midrise buildings (3–9 stories). Few or no trees. Land cover mostly paved. Stone, brick, tile, and concrete construction materials.	 <p>B. Scattered trees</p>	Lightly wooded landscape of deciduous and/or evergreen trees. Land cover mostly pervious (low plants). Zone function is natural forest, tree cultivation, or urban park.
 <p>3. Compact low-rise</p>	Dense mix of low-rise buildings (1–3 stories). Few or no trees. Land cover mostly paved. Stone, brick, tile, and concrete construction materials.	 <p>C. Bush, scrub</p>	Open arrangement of bushes, shrubs, and short, woody trees. Land cover mostly pervious (bare soil or sand). Zone function is natural scrubland or agriculture.
 <p>4. Open high-rise</p>	Open arrangement of tall buildings to tens of stories. Abundance of pervious land cover (low plants, scattered trees). Concrete, steel, stone, and glass construction materials.	 <p>D. Low plants</p>	Featureless landscape of grass or herbaceous plants/crops. Few or no trees. Zone function is natural grassland, agriculture, or urban park.
 <p>5. Open midrise</p>	Open arrangement of midrise buildings (3–9 stories). Abundance of pervious land cover (low plants, scattered trees). Concrete, steel, stone, and glass construction materials.	 <p>E. Bare rock or paved</p>	Featureless landscape of rock or paved cover. Few or no trees or plants. Zone function is natural desert (rock) or urban transportation.
 <p>6. Open low-rise</p>	Open arrangement of low-rise buildings (1–3 stories). Abundance of pervious land cover (low plants, scattered trees). Wood, brick, stone, tile, and concrete construction materials.	 <p>F. Bare soil or sand</p>	Featureless landscape of soil or sand cover. Few or no trees or plants. Zone function is natural desert or agriculture.
 <p>7. Lightweight low-rise</p>	Dense mix of single-story buildings. Few or no trees. Land cover mostly hard-packed. Lightweight construction materials (e.g., wood, thatch, corrugated metal).	 <p>G. Water</p>	Large, open water bodies such as seas and lakes, or small bodies such as rivers, reservoirs, and lagoons.
 <p>8. Large low-rise</p>	Open arrangement of large low-rise buildings (1–3 stories). Few or no trees. Land cover mostly paved. Steel, concrete, metal, and stone construction materials.	VARIABLE LAND COVER PROPERTIES	
 <p>9. Sparsely built</p>	Sparse arrangement of small or medium-sized buildings in a natural setting. Abundance of pervious land cover (low plants, scattered trees).	Variable or ephemeral land cover properties that change significantly with synoptic weather patterns, agricultural practices, and/or seasonal cycles.	
 <p>10. Heavy industry</p>	Low-rise and midrise industrial structures (towers, tanks, stacks). Few or no trees. Land cover mostly paved or hard-packed. Metal, steel, and concrete construction materials.	<p><i>b. bare trees</i></p> <p><i>s. snow cover</i></p> <p><i>d. dry ground</i></p> <p><i>w. wet ground</i></p>	<p>Leafless deciduous trees (e.g., winter). Increased sky view factor. Reduced albedo.</p> <p>Snow cover >10 cm in depth. Low admittance. High albedo.</p> <p>Parched soil. Low admittance. Large Bowen ratio. Increased albedo.</p> <p>Waterlogged soil. High admittance. Small Bowen ratio. Reduced albedo.</p>

Figure 2.3: Local climate zones classification scheme and 17 standard classes with brief definition (Stewart and Oke in 2009). © Copyright 2012 AMS.

Numerous researchers are using this LCZ method as their standard classification approach for the urban structure types for climate studies to describe the impact of urbanization on LST distribution. For example, Middel (Middel et al., 2014) examined LST of urban types during the mid-afternoon microclimate in Phoenix, Arizona applying the LCZ method. In another study Simanjuntak (Simanjuntak et al., 2019) created an LCZ map for Bandung, Indonesia, at a local level, using high resolution SPOT image using object based image analysis (OBIA) with an overall accuracy of 69% for the year 2016. Another study conducted in the greater Nancy Area of France (Leconte et al., 2015) used the LCZ schema for UHI measurement by investigating the thermal pattern in a homogeneous urban structure. The findings demonstrated that LCZs provided a detailed and standardized representation of urban structures. This approach enabled the researchers to identify significant temperature variations across different LCZs, highlighting the importance of considering urban structure in UHI studies.

By utilizing LCZs, researchers and urban planners can add to their understanding of urban thermal dynamics, UHI effects more precisely, and develop targeted strategies to improve urban climate resilience (G. Chen et al., 2023). LCZs offer a detailed classification system that accounts for building height, density, surface cover, and thermal properties, which are crucial for accurately modeling and analyzing the UHI effect. This level of detail helps in identifying specific urban characteristics that contribute to increased heat retention and variability in urban areas.

Mapping LCZs globally, however, presents significant challenges. While Bechtel (Bechtel et al., 2015) has made substantial progress in creating global LCZ maps, these maps often lack local accuracy due to the limitations of high-resolution data sources (Yang et al., 2020; Ma et al., 2021). Mapping building height, size, and density with such data can be particularly challenging, leading to potential inaccuracies in the classification of urban zones. High-resolution datasets and local validation are essential to improve the accuracy of LCZ mapping (Simanjuntak et al., 2019; Yang et al., 2020).

In recent years, the use of LCZs has increasingly focused on city scales for climate model simulations, analyzing the thermal behavior of various urban land features in connection with the UHI effect (Danylo et al., 2016; Han et al., 2020; Wei & Sobrino, 2024).

For our study, we selected two cities in India with different Köppen climate classifications and used LCZs to quantify LST results, allowing us to compare the thermal environments of cities of varied sizes. We have used a fusion strategy where we first generate regular LULC using Landsat-8 data (30m) then fused its impervious class with freely available global LCZ map (100m) to extract and remap only urban classes (built-type in Figure 2.3) based on global LCZ. The classification and re-mapping procedures are explained with details in the data and methods section.

3. STUDY AREA

For this study, we selected two cities in the Indian state of Gujarat. Gujarat is located on the west coast of India, bordering the Arabian Sea. The two cities of interest are Ahmedabad and Surat city (Figure 3.1).



Figure 3.1: Location map of the study area, Ahmedabad and Surat, zoom imagery taken from Esri, Maxar, World imagery

Gujarat has a rapidly growing population and significant urban growth. As per the 2011 census, the population of Gujarat is approximately 60.5 million. The state has experienced a notable population growth rate of 19% over the past decade, with urbanization playing a significant role. Around 42.60% of Gujarat's population resides in urban areas, reflecting the state's increasing urbanization (Census 2011 India). The urban population growth in Gujarat was about 36% between 2001 and 2011 and is expected to continue rising (Census 2011 India). This urban expansion is evident in cities like Ahmedabad and Surat, which are among the largest urban centers in the state, making them major urban hubs with substantial contributions to the state's overall urbanization.

These cities fall under different Köppen climate classifications, providing a unique opportunity to compare the impact of climate on LST and UHI. Ahmedabad has a hot semi-arid climate, while Surat has a tropical savanna climate. Studying these variations helps in understanding how local climate influences urban thermal dynamics.

3.1. Ahmedabad City

Ahmedabad is one of the largest urban agglomerations in India and the largest city in Gujarat situated along the banks of Sabarmati River. The city spans an area of around 525 square kilometers with a population of approximately 7.3 million people. It falls under the Köppen climate classification "BSh," representing hot semi-arid climate (Peel et al., 2007). Its summer is extremely hot with temperatures exceeding 40°C in May-June (Figure 3.2), making it one of the hottest cities in India. Winters are mild to warm, with temperatures ranging from 10°C to 25°C in January, which is the coldest month. Ahmedabad receives its rainfall during the monsoon season (June to September). During this season, the city receives heavy showers and thunderstorms with approximately an average monthly precipitation of 300mm during the months of July and August (Figure 3.3). Ahmedabad can be very humid during the monsoon season, making the weather feel hotter than the actual temperatures. On the other hand, during the dry season, the humidity is relatively low.

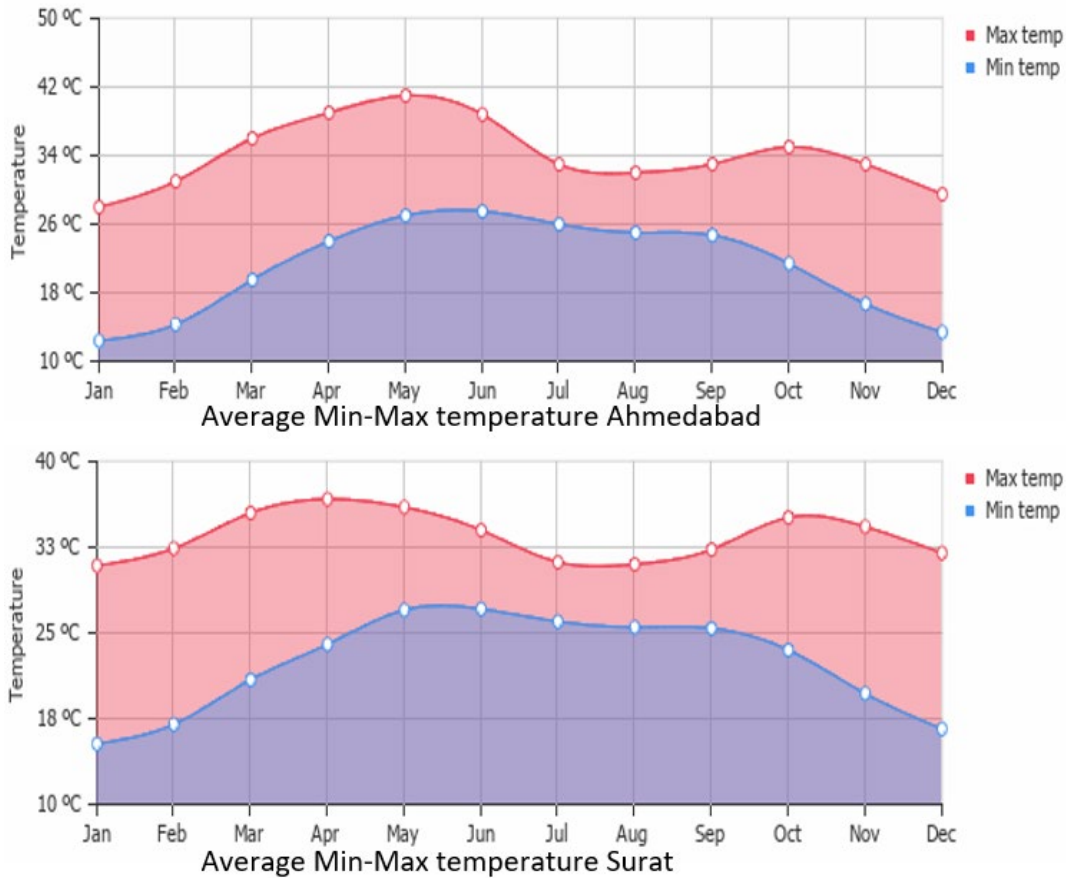


Figure 3.2: Average minimum and maximum temperature in Ahmedabad and Surat cities, © Copyright 2022 weather-and-climate.com

3.2. Surat City

Another study area we selected is Surat in the Indian state of Gujarat. The city spans an area of around 330 square kilometers with a population of approximately 6.0 million people. It falls under the Köppen climate classification "Aw," which denotes a tropical wet and dry or savanna climate (Peel et al., 2007), and it borders the Arabian sea. The summers in Surat are hot, especially from March to June, with temperatures reaching around 35°C to 37°C, which is slightly less than in Ahmedabad (Figure 3.2). The hottest months are April and May, unlike Ahmedabad, where the hottest months are May to June. Winters in Surat are mild and pleasant, with temperatures ranging from 15°C to 30°C, which is generally warmer than in Ahmedabad, with January being the coldest month. Surat receives higher monsoon rainfall than Ahmedabad (Figure 3.3).

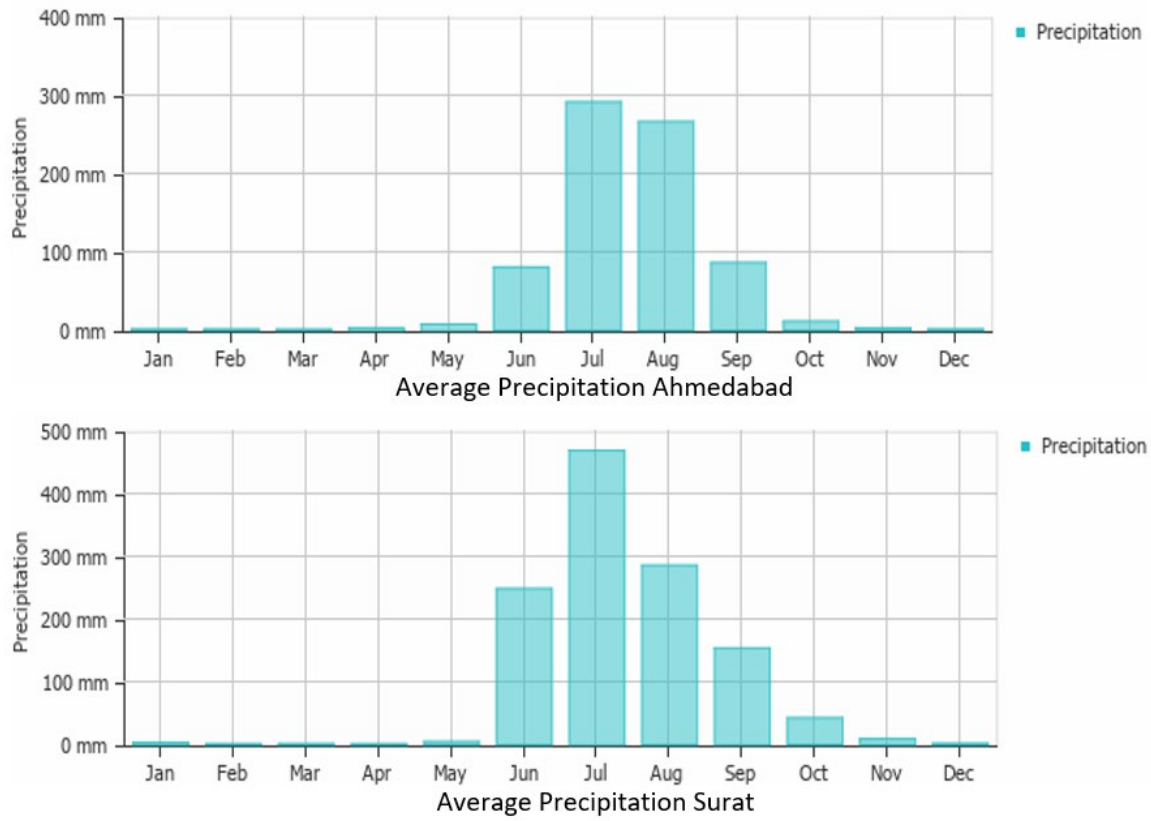


Figure 3.3: Average precipitation in Ahmedabad and Surat city,
 © Copyright 2022 weather-and-climate.com

4. DATA AND METHODOLOGY

This chapter explains the methods and data used to address the research objectives. It first outlines the general conceptual framework of the research methodology followed by the details of data used for this research. It also provides information about the analyses that were conducted to achieve the research objectives.

4.1. General Framework

As mentioned in the introduction section, it is important to discriminate heterogeneous urban surface patterns to identify localized effects on the SUHI. Here we generated a land cover map that has a single impervious surface class using Landsat data. Then we used a global LCZ dataset to replace our classified impervious surfaces with more detailed LCZ urban classes (classes 1 to 10 mentioned in Figure 2.3). Finally, this fused LCZ dataset was used to study relationships with LST (General research framework Figure 4.1).

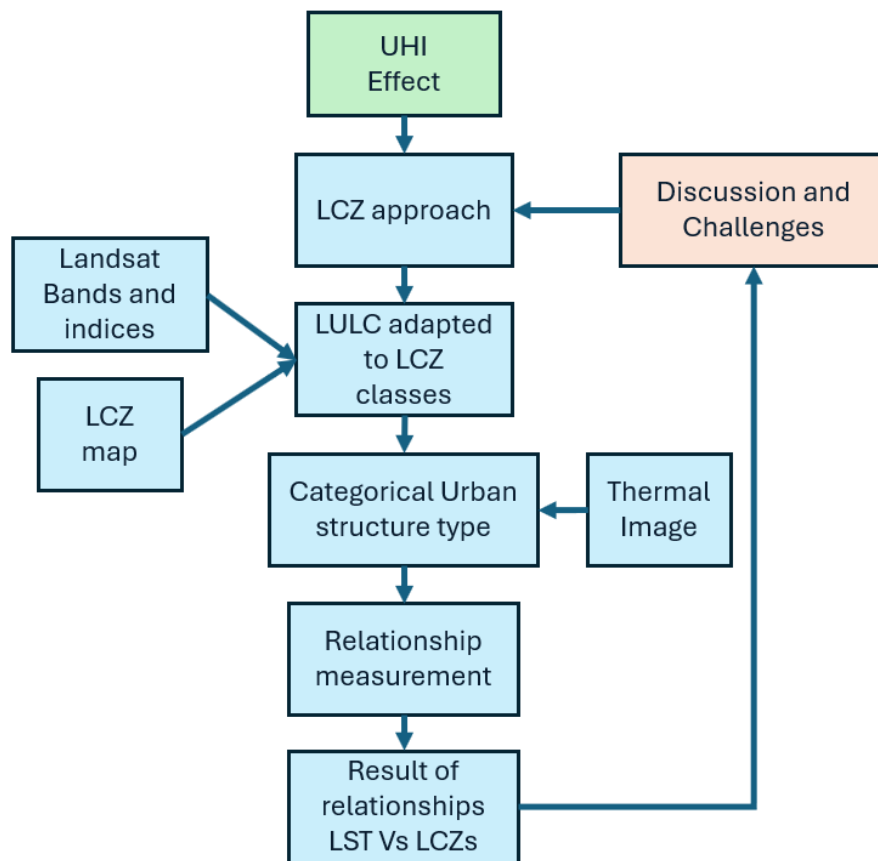


Figure 4.1: General framework of the research

4.2. LULC map production and Fusion with LCZ map

Initially, the LULC maps of both study sites were produced using Landsat-8 (LS-8) data from 2020. For this purpose, 452 training points for Ahmedabad and 382 training points for Surat were manually collected using Google Earth images from 2020. These points were used to classify each city into five base classes: *Impervious, Bare soil, Trees, Herb/Crop, and Water* using the Random Forest classification method in Google Earth Engine.

The Landsat-8 data, filtered to include less than 5% cloud cover, produced a stack of 23 images for Ahmedabad and 15 images for Surat. Several indices were generated using various bands of the LS-8 data, which served as additional input features for the classification model. Details of these bands and indices are listed in Table 1.

Next, a reducer with the 75th percentile was applied to the combined stack of LS-8 images and the calculated indices for each study area, resulting in a composite multiband image for each city. These composite images were then used to train a Random Forest classifier, which subsequently generated the classification maps for each city.

Table 4.1: List of Input features fed to random forest classifier.

LS-8 bands / Indices used	Band spectrum / Expression of Indices
Band -1 to Band -7	Ultra Blue, Blue, Green, Red, Near-Infrared (NIR), Shortwave infrared 1 (SWIR_1), Shortwave infrared 2 (SWIR_2)
NDVI	Normalized Difference Vegetation Index $(\text{NIR} - \text{Red}) / (\text{NIR} + \text{Red})$
EVI	Enhanced Vegetation Index $2.5 * ((\text{NIR} - \text{Red}) / (\text{NIR} + 6 * \text{Red} - 7.5 * \text{Blue} + 1))$
LSWI	Land Surface Water Index $(\text{Green} - \text{NIR}) / (\text{Green} + \text{NIR})$
NDBI	Normalized Difference Built-up Index $(\text{SWIR}_2 - \text{NIR}) / (\text{SWIR}_2 + \text{NIR})$
NDWI	Normalized Difference Water Index $(\text{NIR} - \text{SWIR}_1) - (\text{NIR} - \text{SWIR}_2)$

The validation process for both Ahmedabad and Surat involved comparing the classification results with a set of validation points collected for each city. For Ahmedabad, 113 validation points were used, resulting in a validation accuracy of 83% and a Kappa coefficient of 75%. For Surat, 100 validation points were used, resulting in a validation accuracy of 77% and a

Kappa coefficient of 64%. These metrics indicate the effectiveness of the classification method in each city. Detailed confusion matrices are presented in appendix 3 & 4.

After generating the LULC map at a resolution of 30m (the same as Landsat-8), we applied a fusion strategy using an existing map based on the LCZ classification scheme. The scheme was initially proposed by Stewart and Oke (Stewart & Oke, 2012) and later Demuzere (Demuzere et al., 2022) produced a global LCZ map to support earth system modeling and urban-scale environmental science. This dataset was produced using multiple Earth observation (EO) datasets from 2018 (EO data set table in appendix 1), has a 100m pixel size and freely accessible through Google Earth Engine. The LCZ scheme includes 17 urban and natural landscape types, as shown in Figure 2.3.

Based on visual inspection of the global LCZ dataset in our study area, we noted that the LCZ data were more focused on urban classes and did not capture all-natural land-cover classes such as trees, crops/herbs, and soil in detail. Also, it sometimes misclassified dense natural vegetation as urban if there were few human settlements nearby. In contrast, our LULC map clearly distinguished urban vegetation as trees or crop/herb land classes, ensuring an accurate representation of urban vegetation. With a 30m resolution and overall accuracy of over 75%, our map also precisely mapped impervious surfaces.

To integrate both datasets effectively, we implemented a fusion strategy where the impervious class in our LULC map was reclassified based on the LCZ's urban built type classes (Figure 2.3). We remapped each pixel of the impervious class to the corresponding LCZ built type class. If the corresponding LCZ was not a built type, it was considered a misclassification and replaced with the sparsely built class, assuming a mix of natural and urban features. This fusion and remapping concept is illustrated in Figure 4.2. This approach ensures that all natural classes (except impervious) remain intact while enhancing the urban classification with detailed LCZ types, providing a more comprehensive and accurate representation of the study areas. The output of each classification map and the fused map for Ahmedabad city is shown in Figure 4.4 for reference.

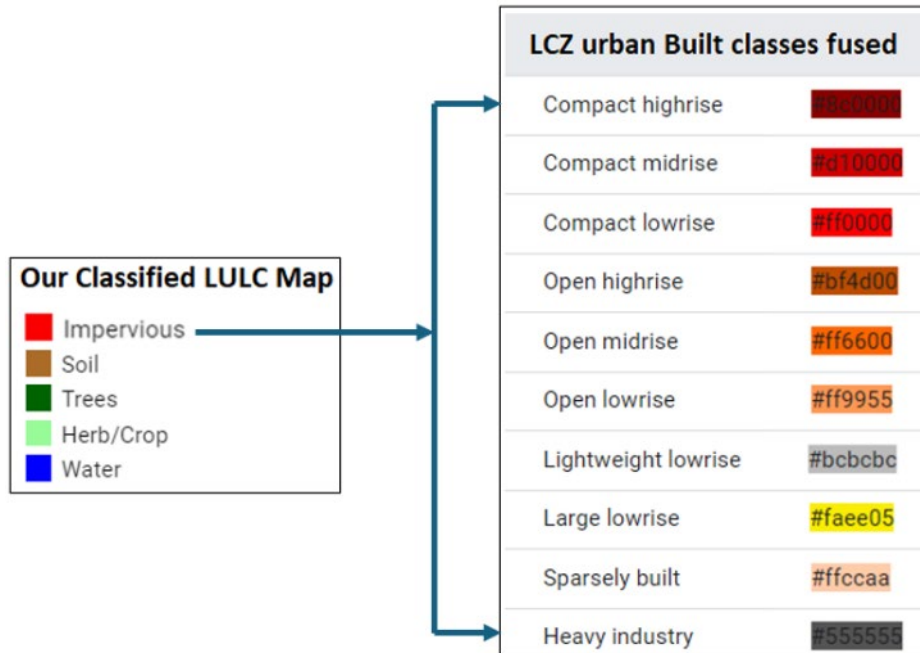


Figure 4.2: LULC remapped schema to fuse with LCZ urban built classes

Finally, for analysis purposes, we selected six LCZ classes: 'Compact midrise', 'Compact low rise', 'Open low rise', 'Large low rise', 'Trees', and 'Crops/Herbs'. These classes were chosen because they cover significant areas and are hypothesized to have strong effects on LST in the study area. Overall classes obtained after fusion can be seen in Figure 4.3 where classes under analysis are marked with star signs.



Figure 4.3: Classes obtained after fusion (remapping), and classes under analysis are marked with star

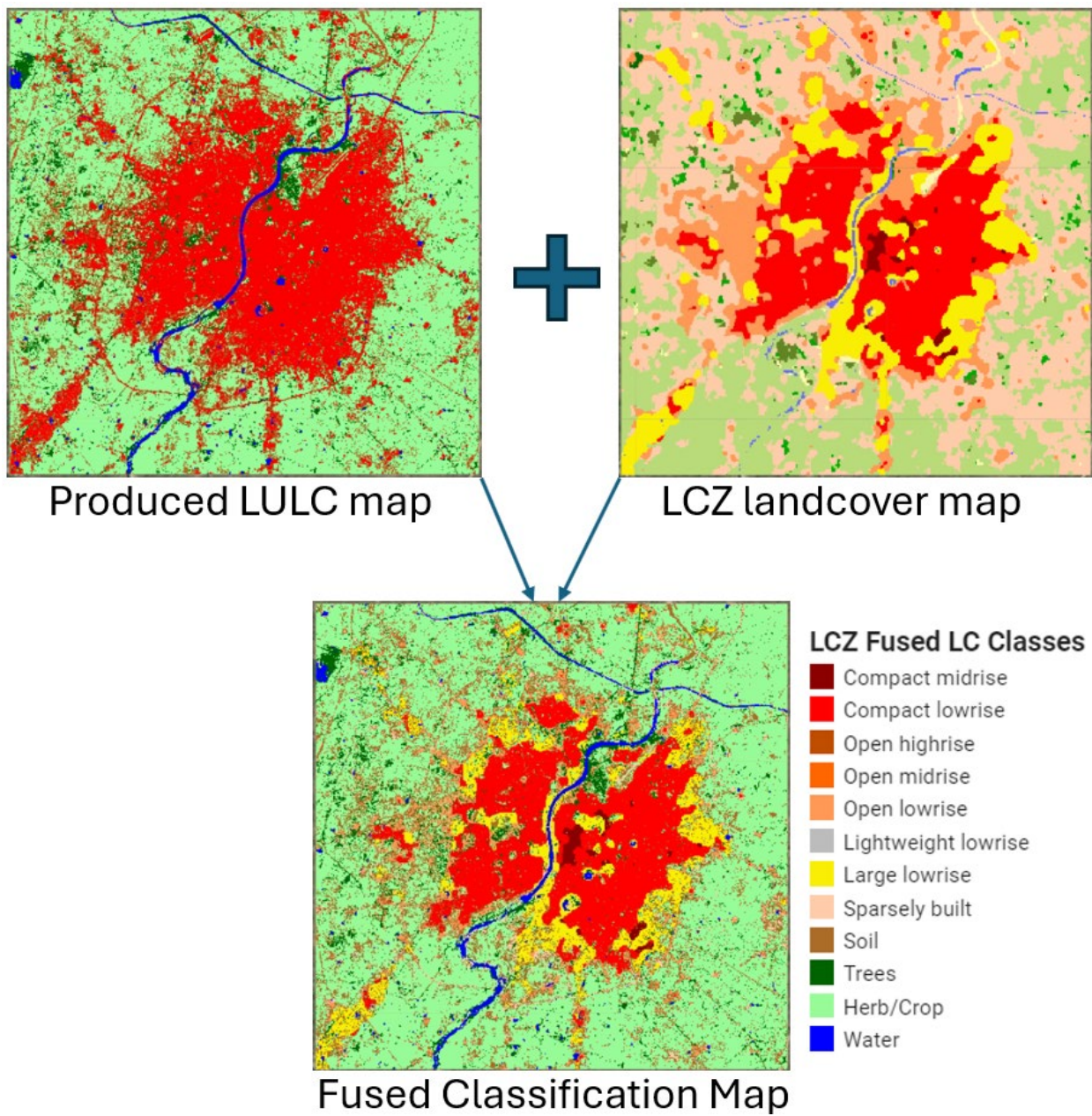


Figure 4.4: LULC remapped with LCZ map to produce a fused map for Ahmedabad city

4.3. ECOSTRESS data and processing

Ecosystem Spaceborne Thermal Radiometer Experiment on Space Station (ECOSTRESS) is an experimental instrument onboard the International Space Station (ISS) on June 29th, 2018. Its native spatial resolution is 38 m × 68 m with a swath width of 402 km and a revisit time of about 3 to 5 days at different times of day depending on the latitude (Hulley et al., 2019). The observed LST data are then aggregated to 70m × 70m pixel resolution as higher-level products. The primary purpose of this satellite is to monitor plant water content and stress in the vegetation, with application to agriculture pertaining to water consumption use. However, its LST data are valuable for research on other thermal phenomena such as the SUHI. They are especially well suited for urban studies because of being freely available high-resolution data (70m), with LST observations across the entire diurnal cycle. Due to its five thermal bands, ECOSTRESS allows for the implementation of multispectral temperature/emissivity separation approaches for retrieving the most accurate LST over urban (Hulley et al., 2019).

ECOSTRESS LST data can be obtained from the NASA *Land Processes Distributed Active Archive Center* (NASA-LPDAAC). We used *Application for Extracting and Exploring Analysis Ready Samples* (AppEEARS), an interactive web-portal that allows to select a region of interest (ROI) and desired period of data to download, and later provides an email link to download the ordered data. For our study area, we downloaded data as mentioned in table 2 for the period of September 2018 to March 2024.

Table 4.2: Details of the downloaded ECOSTRESS data using AppEEARS portal.

ECOSTRESS data (Level -2)	Data information and its use
ECO2LSTE Version 1 Land Surface Temperature (SDS_LST)	Atmospherically corrected Land Surface temperature in Kelvin
ECO2LSTE Version 1 Quality Control for LST (SDS_QC)	Quality Control for LST and emissivity
ECO2CLD Version 1 Cloud Mask (SDS_Cloud Mask)	Provides cloud mask for ECO2LSTE data

A detailed flow chart is presented in Figure 4.5 describing the overall processing steps. Most processing and analysis were conducted using R scripts. However, we also used ArcGIS for

data visualization and some manual geo-referencing. (Refer appendix 2 for detailed list of downloaded and used data for this study)

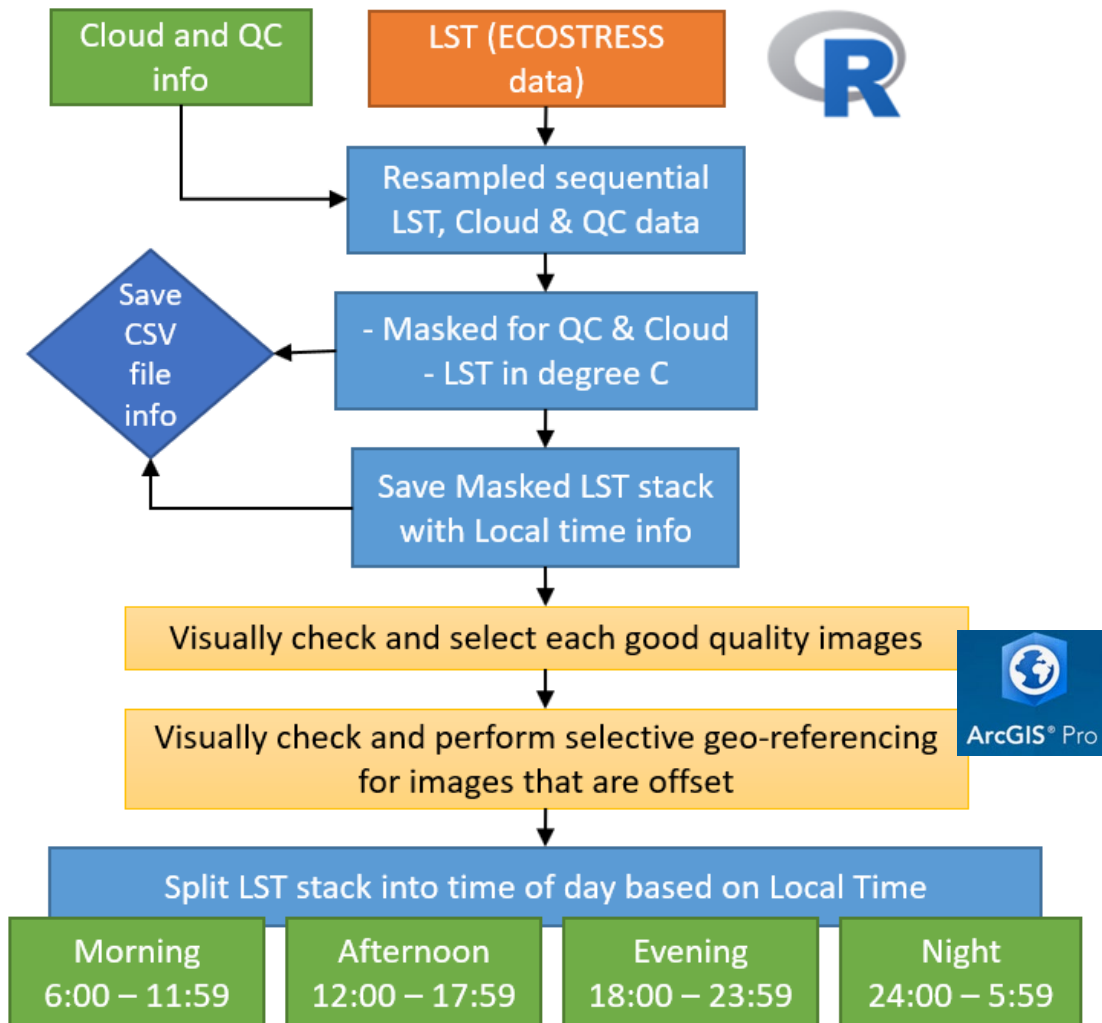


Figure 4.5: Flow chart representing the data processing using R on ECOSTRESS data to extract cloud free and of better quality. Orange box section was done manually using ArcGIS Pro

Initially, ECOSTRESS LST data, along with cloud and quality control (QC) information, were collected. These datasets were sequentially resampled to ensure alignment on a common grid. Cloud and QC masking were then applied to filter out areas affected by clouds and quality issues, converting the LST data into degrees Celsius. The resulting masked LST stack, which included local time information, was saved for future processing steps.

Following this, a quality assessment of the data was conducted visually. Each image within the masked LST stack was visually inspected to ensure high quality cloud-free images were selected. Some images exhibited spatial offsets of a few pixels and were subjected to geo-referencing to correct their alignment. For this alignment manual control points were generated referencing misaligned spatial features with satellite image on ArcGIS. One of the misaligned images with control points is presented in Figure 4.6 for reference.

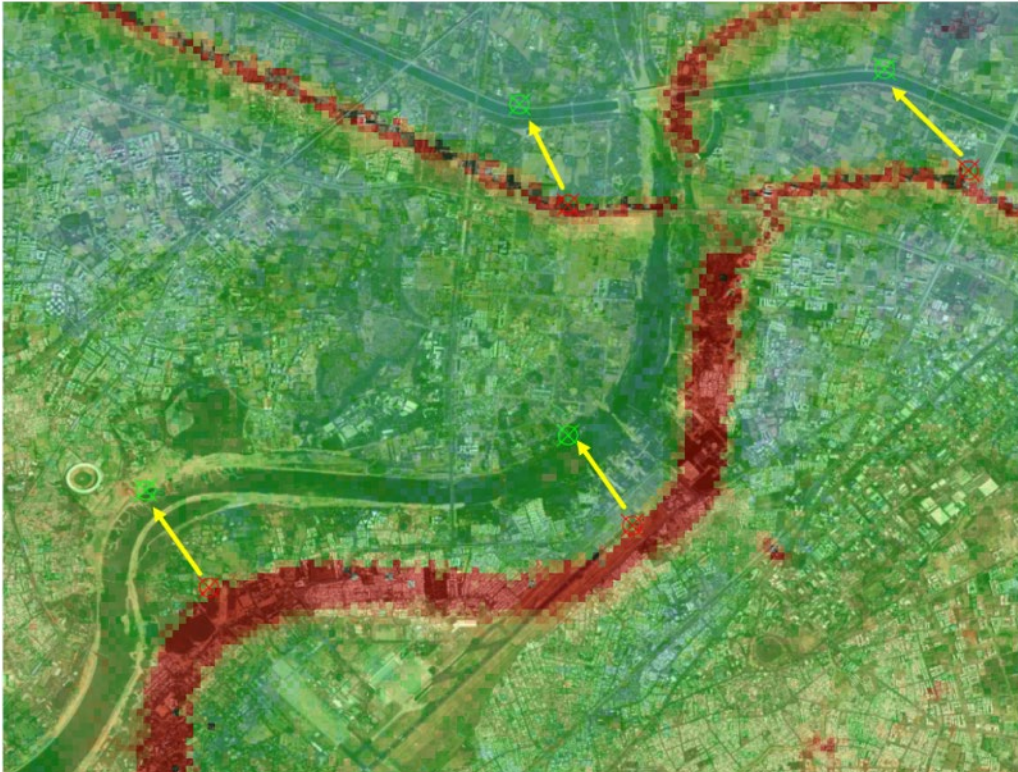


Figure 4.6: Screen shot of ArcGIS Pro showing a misaligned ECOSTRESS data along with manually selected control points to guide the alignment process, while referencing the satellite image on the background

Next, images were divided into four distinct time-of-day categories based on local time: Morning (6:00 - 11:59), Afternoon (12:00 - 17:59), Evening (18:00 - 23:59), and Night (00:00 - 5:59). This segmentation allows for detailed temporal analysis of LST variations. Finally, all the LST data (2018-2024) were divided into two seasons to compare the seasonal variations among the classes. Seasons are namely Summer (Mar-Apr-May-Jun), and Winter (Oct-Nov-Dec-Jan-Feb). Each season consists of 4 averaged diurnal periods. The monsoon period (July-August-September) was excluded from the analysis due to insufficient data. During these

times, the study area was predominantly covered by clouds, which obstructed the collection of reliable LST data. (Please refer to Appendix 2 for data availability tables)

4.4. Data Analysis

4.4.1. Monthly LST trend analysis

We generated a monthly stack of LST data from ECOSTRESS covering both cities and used them to study monthly LST trends for both cities. The monthly LST for each city was calculated as mean LST values from all cloud-free 70m pixels within the city limits, manually delineated using nighttime light data from the VIIRS Stray Light Corrected Nighttime Day/Night Band Composites in Google Earth Engine (Figure 4.7). These monthly LST values were used to calculate the monthly trend of LST from both cities and compare against each other to understand their monthly behavior and associations with the monthly air temperature.

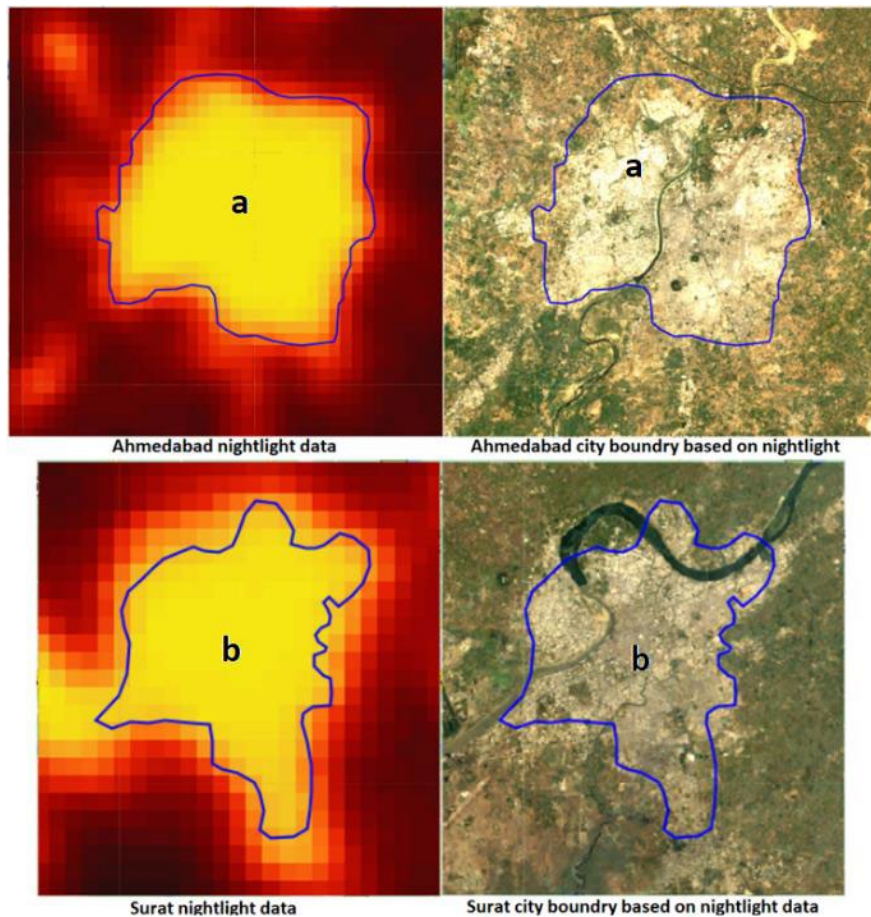


Figure 4.7: Ahmedabad city boundary 'a' and Surat city boundary 'b' shown as blue polygons overlaid over Nighttime light data from VIIRS and Google Map

4.4.2. Descriptive analysis of LST spatial patterns

We visually inspected hotspot zones during summer afternoons when temperatures are expected to peak. This analysis focuses on identifying areas with high LST and their corresponding land cover LCZ classes. Additionally, we compared temperature differences between well-vegetated and non-vegetated areas to assess the cooling effect of vegetation. This involved selecting representative vegetated and non-vegetated zones within the city and analyzing their respective LST values. The cooling effect was quantified by the temperature reduction observed in vegetated areas compared to their non-vegetated counterparts. This comparison highlighted the role of urban green spaces in mitigating high temperatures and reducing the UHI effect.

4.4.3. Quantitative analysis of relationships between LST and LCZs

Here we analyzed the relationships between LST and each LCZ-fused land cover class, quantifying variations across different seasons and diurnal periods, from morning to night. This analysis revealed temperature changes for each land cover type and their responses to seasonal and diurnal shifts. We presented these variations using box plots that displayed 25th and 75th percentiles, and median LST values for each land cover type.

These box plots were created using the fused land cover map and LST data. The land cover map has a 30m resolution, while the LST data has a 70m resolution. To ensure consistent pixel size and count before generating the box plots, each LST data point was resampled using bilinear interpolation to a 30m resolution based on the land cover map. Then, grouped box plots were created for each land cover class, displaying the corresponding LST values for each diurnal period.

4.4.4. Quantitative analysis of LST gradient from city core to edge

In this analysis, we examined the temperature gradients from the city center to the outskirts. This involved assessing the relationship between temperature and distance from the centroid of the city boundary. We generated scatter plots and conducted linear regression analysis of LST versus distance for each season and diurnal period in both cities.

To achieve this, we selected 1000 random points within the study area and extracted LST values for each season and diurnal cycle. Then we created a Euclidean distance survey over the study area and extracted the distance value of each random point from the city center. The random points and city centroid for Ahmedabad are shown in Figure 4.8.

To obtain accurate geographical distances, it was essential to use the correct projection and coordinate system. For this analysis, we utilized the WGS 84 ellipsoid with the Gujarat coordinate system (EPSG:7761). This system was applied to all LST and Euclidean distance raster images, ensuring precise distance measurements for the analysis.

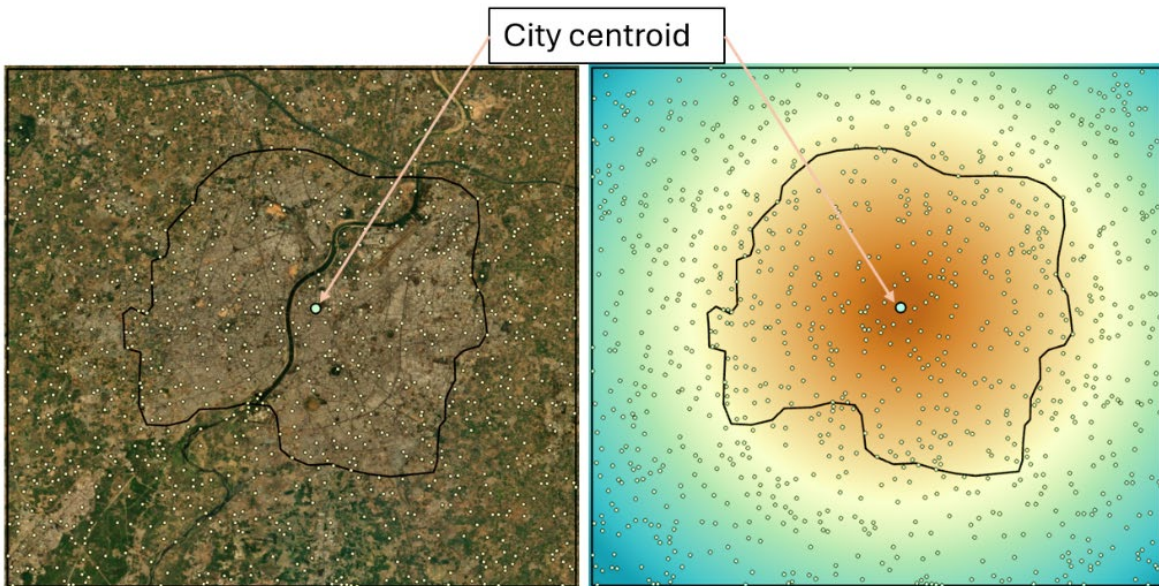


Figure 4.8: Displaying 1000 random points along with the centroid over Ahmedabad. Satellite image as background (left). Euclidean distance as background (right)

5. RESULTS

5.1. Average monthly LST

The monthly trends of LST over both cities are shown in Figure 5.1. Depending upon the month, the number of available satellite observation data varies (table in Appendix 2).

The comparison of monthly LST for both the cities revealed different seasonal variations in the temperature profile. During the winter months (December and January), Surat was notably warmer than Ahmedabad, generally about 5° C higher. Both cities experienced a significant rise in LST during the spring (March, April, and May), but Surat reached a peak of approximately 40°C in April, higher than Ahmedabad's 35°C. In early summer, Ahmedabad continued to heat up, peaking at 45°C in June, while Surat's temperatures stabilized around 38°C in June after reaching a peak LST in April and May.

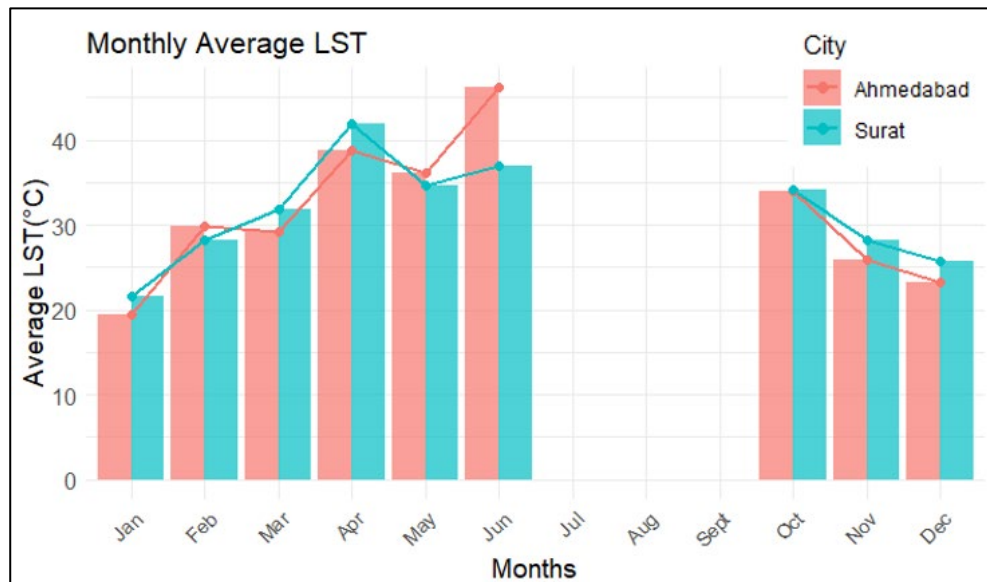


Figure 5.1: Monthly average LST trend of two cities, Ahmedabad and Surat

LST observations were not available between July and September because of high cloud cover during the monsoon. After the monsoon in October, both the cities showed a similar cooling pattern, with temperatures dropping to around 35°C. However, as late autumn transitioned to winter in November and December, Ahmedabad cooled more rapidly, with November temperatures around 25°C compared to Surat's 30°C.

The LST observations, despite being collected from a limited number of scenes from the ECOSTRESS satellite, closely resemble the seasonal trends in monthly air temperatures (Figure 3.2, chapter 3 Study area). Notably, Surat's maximum air temperature peaked in April, earlier than Ahmedabad's peak in June. Additionally, the data showed that Surat was generally warmer than Ahmedabad during the winter and autumn seasons.

5.2. Visual interpretation of LST hotspots and urban structures

We visually interpreted the localized spatial patterns of LST hotspots in both cities and assessed their associations with urban structures or settlement types. Figures 5.2 (for Ahmedabad City) and 5.3 (for Surat City) illustrate multiple images of each hotspot with zoom images. The LST images used for this interpretation were calculated as the pixel-level means using data for all of the summer months in the afternoon (March, April, May, and June). For clarity in identifying hotspots, only temperatures over 42°C were displayed.

In Figure 5.2, we assessed four hotspots over Ahmedabad City, each ranging from 48 to 52°C. Hotspot 'a' was identified as an international airport, clearly showing its runway and other airport buildings. These locations reached up to 52°C during the summer season, while its surroundings, classified as a 'compact low rise' urban area, were cooler by 5 to 8°C.

The next hotspot, 'b,' was an industrial area identified by its roof size and structures. These roofs were mostly made of metal sheets or a combination of metal sheets and concrete, with heat retaining capacity. Additionally, many of these industries had exhaust chimneys that released more heat into the surroundings. Unfortunately, our LCZ map failed to accurately distinguish these industrial areas, classifying them as compact low rise to large low rise urban classes. These areas lacked any kind of vegetation, and the outskirts of these industrial zones were covered by compact and large low-rise residential areas. Consequently, the temperature did not vary much and remained between 48 to 51°C.

The 'c' hotspot in Figure 5.2 was a huge landfill site forming a hill full of decomposing trash, just at the south-west edge of the city. This place has continual burning spots and was usually hotter than its surroundings, ranging from 48 to 50°C. The surrounding area of the landfill was an urban settlement of compact and large low rise, but the temperature in these areas was 4 to 5°C less than the landfill site.

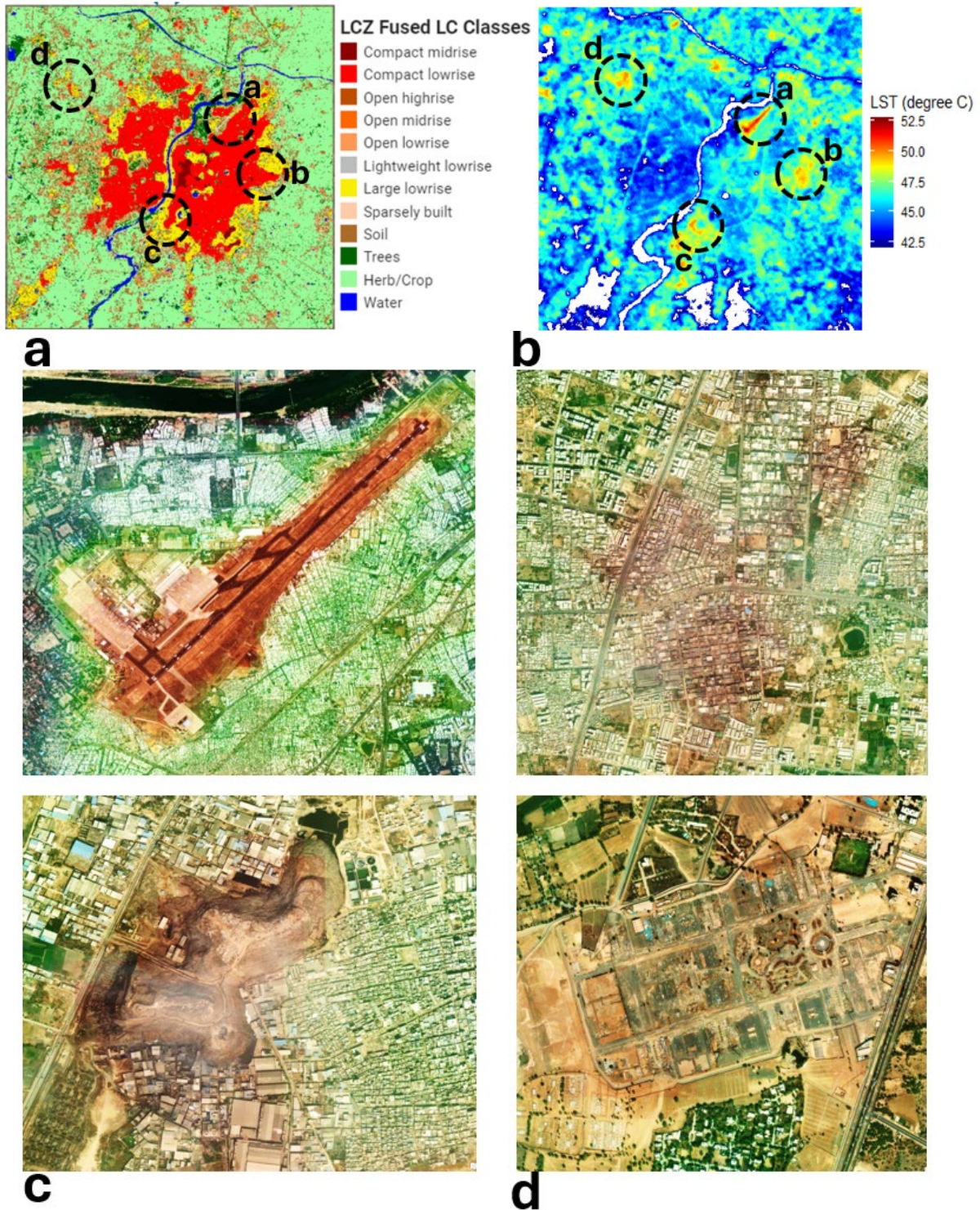


Figure 5.2: Ahmedabad city, Land cover map (top left), Summer (March-June) average LST from ECOSTRESS (top right). 4 zoomed images of hotspot zone a, b, c, and d taken from Esri, Maxar, World imagery (bottom 4)

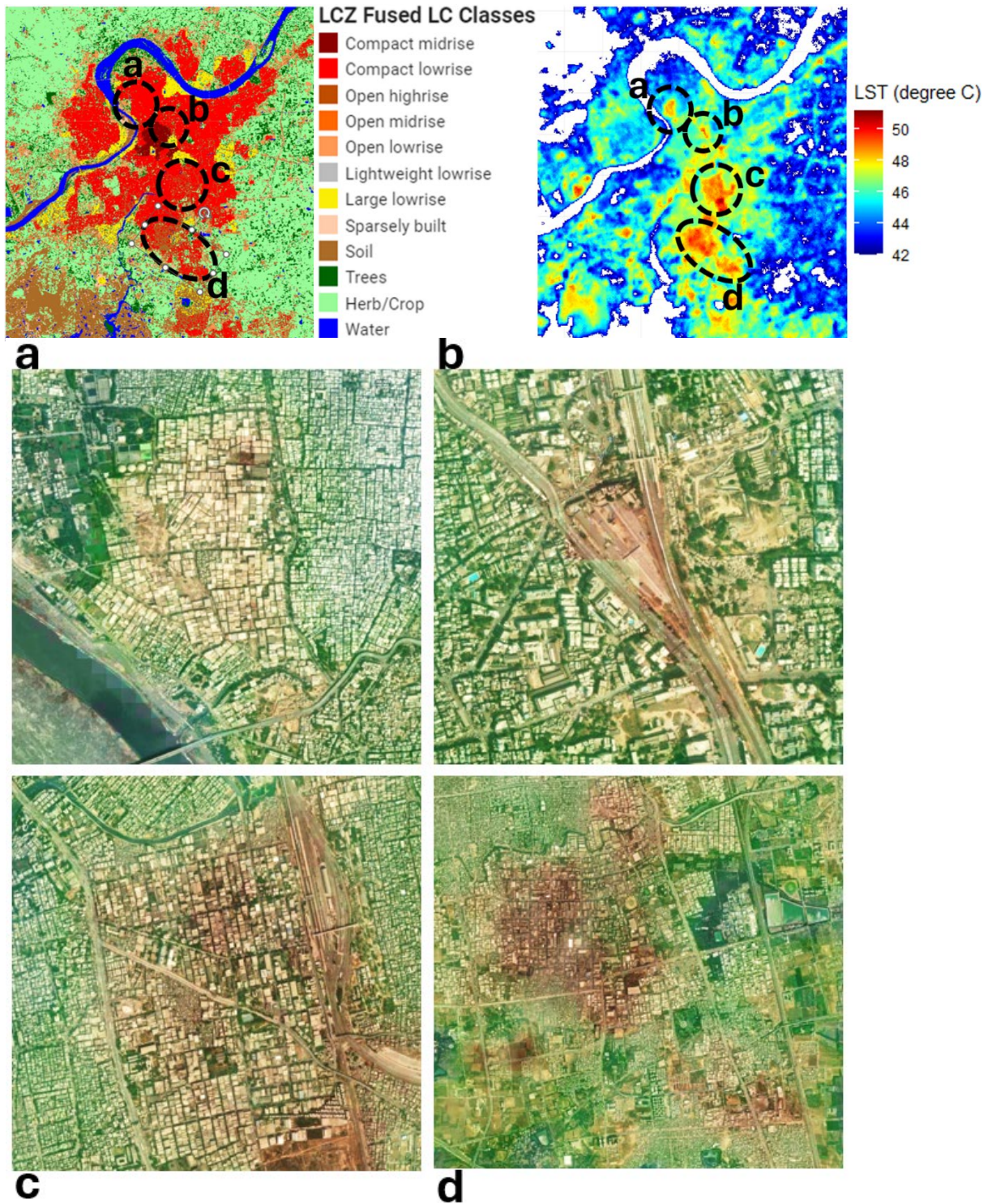


Figure 5.3: Surat city, Land cover map (top left), Summer afternoon (March-June) average LST from ECOSTRESS (top right). 4 zoomed images of hotspot zone a, b, c, d taken from Esri, Maxar, World imagery (bottom 4)

The 'd' hotspot was not within the city boundary and lay north-west of city area. It was loosely connected with the urban fabric by expanding small towns and residential complexes along the connecting roads. This was a large semi-paved area of bare land with exposed soil classified as 'sparsely built,' 'Soil,' and 'Herb/Crop' land cover classes. However, this area radiated significant heat ranging from 48 to 50°C.

Similarly, in Surat City (Figure 5.3), we observed four hotspots ranging from 47 to 50°C. These hotspots were primarily small to large industrial areas spread across the center to the southern border of the city. Unfortunately, our LCZ map categorized these areas as 'compact mid or low rise' to 'large low rise.' However, these zones significantly dominated as hotspot areas. Zones 'a,' 'c,' and 'd' were industrial areas with temperatures ranging from 47 to 50°C. These three hotspots were highlighted due to their larger area, but there were several other smaller industrial areas in Surat with similar LST ranges. Hotspot 'b,' in contrast, was a large, paved area in the center of the city featuring multi-lane roads to the west and train tracks to the east, along with a large train and bus station. This hotspot also exhibited LSTs ranging from 47 to 50°C.

In general, the visual inspection revealed some peculiar hotspots within the city boundary that are mostly dominated by industrial areas and large paved areas, and a landfill site in the case of Ahmedabad city. These areas during the afternoon of summer season exhibited LST between 48 to 52°C. Apart from these peculiar high-LST hotspots, we also found residential areas reaching high temperatures. For example, the 'compact midrise' zones in the city centers of both Ahmedabad and Surat showed temperatures ranging from 45 to 48°C. However, residential areas with some amount of vegetation or forested areas within the city exhibited temperatures ranging from 40°C to 45°C. For example, Figure 5.4 shows a residential area in Surat City with dense vegetation, radiating a temperature of approximately 40°C. The surrounding areas were hotter by 4 to 8°C, particularly the open and dry bare ground, which exhibited an LST of about 48°C during a summer afternoon.

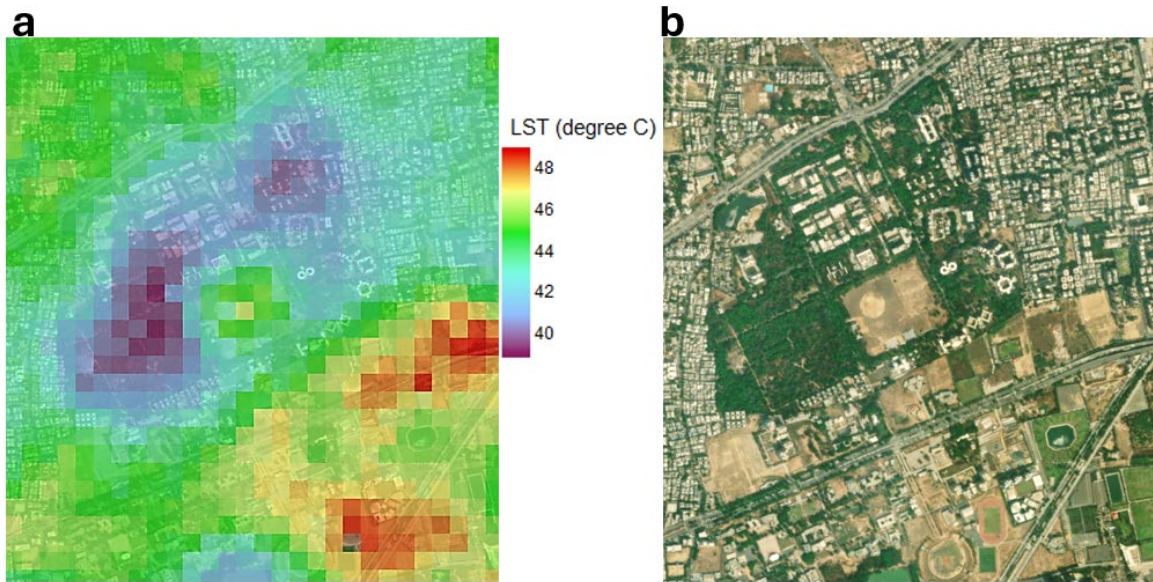


Figure 5.4: Semi-transparent LST image over highly vegetated residence and its urban surrounding (a). Very-high resolution imagery of the corresponding region (b).

5.3. Diurnal LST relationship with LCZ classes

Figures 5.5 and 5.6, respectively show grouped box plots of summer and winter LSTs for each LCZ class and across the four diurnal periods (morning, afternoon, evening, and night) in both cities.

During the summer mornings in both cities, compact midrise exhibited the highest temperatures ($\sim 33^{\circ}\text{C}$), followed by large lowrise ($\sim 32.5^{\circ}\text{C}$). Compact lowrise and open lowrise were relatively cooler (~ 31 to 32°C), while trees and crops/herbs showed the lowest temperatures (~ 30 to 31°C). As the sun's heat intensified in the afternoon, temperatures in both cities for compact midrise and large lowrise reached approximately 46.5°C , closely followed by compact lowrise and open lowrise (~ 45 to 45.5°C). However, in the afternoon, trees and crops/herbs were hotter in Ahmedabad ($\sim 45^{\circ}\text{C}$) compared to Surat ($\sim 43^{\circ}\text{C}$).

In the summer evenings, temperatures in Surat were generally higher across all classes compared to Ahmedabad, indicating a slower rate of heat dissipation in Surat. The trend of variation in temperature of classes in both the cities remained similar, however in contrast to morning or afternoon, compact lowrise were now equally warm as compact midrise ($\sim 27^{\circ}\text{C}$ for Ahmedabad, $\sim 30.5^{\circ}\text{C}$ for Surat). These were followed by large lowrise ($\sim 26^{\circ}\text{C}$ for Ahmedabad, $\sim 30^{\circ}\text{C}$ for Surat) and open lowrise ($\sim 25^{\circ}\text{C}$ for Ahmedabad, $\sim 29^{\circ}\text{C}$ for Surat).

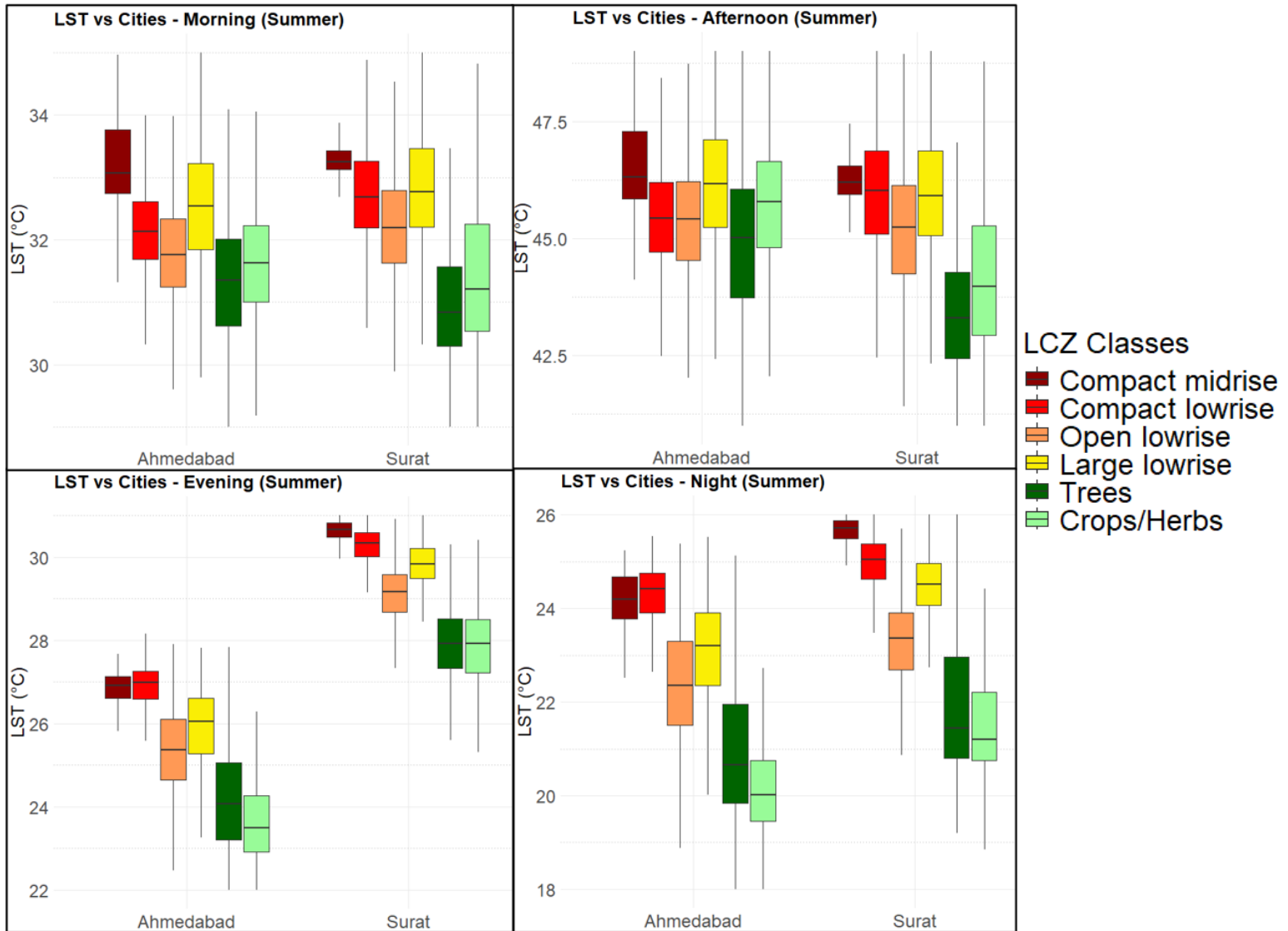


Figure 5.5: Group box plot of LST comparing each city (Ahmedabad and Surat) for different LCZs at different times of the day in summer. Center line in the box represent median, edges of the box represent the first quartile (Q1) and third quartile (Q3), and whiskers represent the range within 1.5 times the interquartile range (IQR) from Q1 and Q3.

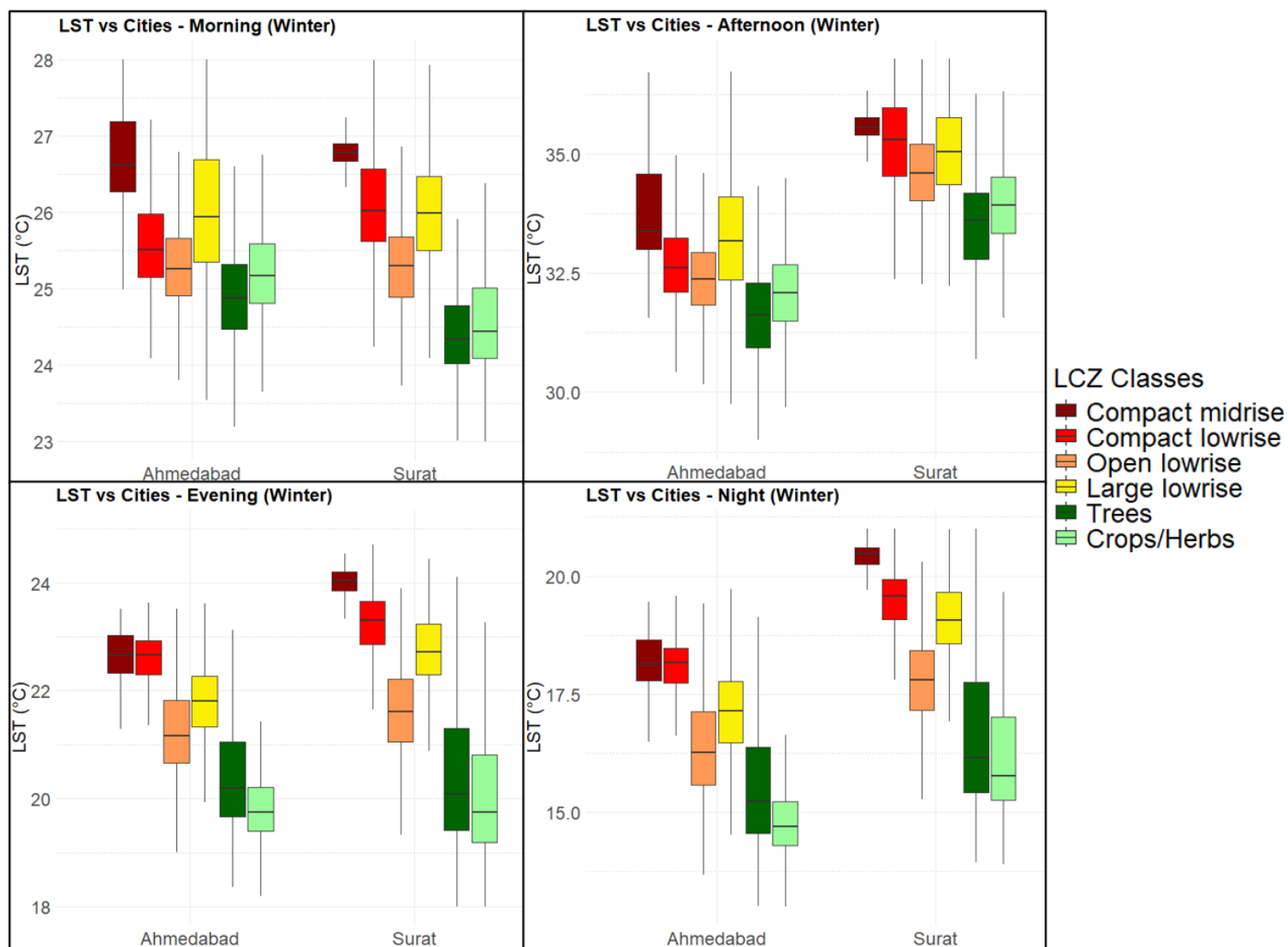


Figure 5.6: Group box plot of LST comparing each city (Ahmedabad and Surat) for different LCZs at different times of the day in winter. Center line in the box represent median, edges of the box represent the first quartile (Q1) and third quartile (Q3), and whiskers represent the range within 1.5 times the interquartile range (IQR) from Q1 and Q3.

Trees and crops/herbs were about $\sim 24^{\circ}\text{C}$ in Ahmedabad, while in Surat, they were about $\sim 28^{\circ}\text{C}$.

During the summer nights, Surat still exhibited slightly higher temperatures compared to Ahmedabad across all classes. However, the temperature variations across different LCZ classes within the cities were similar, except for the compact lowrise class in Surat that exhibited lower LST ($\sim 0.5^{\circ}\text{C}$) than compact midrise. Compact midrise and compact lowrise had the highest temperatures, followed by large lowrise and then open lowrise, again differing from the patterns in morning and afternoon where large lowrise was higher second to compact midrise. At night, trees and crops/herbs showed a $\sim 4^{\circ}\text{C}$ temperature difference compared to other diurnal periods when compared with compact midrise, the hottest class, suggesting that UHI effects were stronger during the night.

In winter, except in the morning, the urban classes in Surat were slightly warmer than those in Ahmedabad. Notably, in summer, Surat was warmer only during the evening and night, while the temperature variation remained similar across all classes throughout the diurnal cycle for each season. For both cities, compact midrise generally had the highest temperatures in both seasons. However, there were differences in temperature trends between large lowrise and compact lowrise classes within the diurnal cycle. During the morning and afternoon, large lowrise exhibited higher temperatures than compact lowrise, while in the evening and night, compact lowrise recorded higher temperatures. Among urban classes, open lowrise had the lowest temperatures across all diurnal cycles. Additionally, trees and crops/herbs were approximately $\sim 2^{\circ}\text{C}$ cooler than the urban classes throughout all diurnal cycles in winter.

5.4. LST gradient analysis

Figures 5.7 and 5.8 depict the relationship between LST and distance from the city center in Ahmedabad and Surat during various times of the day (Morning, Afternoon, Evening, and Night) and seasons (Summer and Winter). These scatter plots were generated from extracting LSTs from 1000 random points within each city with distances calculated using Euclidean distance as described in Chapter 4.4.1. Each plot includes a linear regression line to indicate the trend, along with R^2 values and p-values to highlight the strength and significance of the correlation.

During summer mornings in both cities, there was a negative correlation between LST and distance from the city center. However, during the afternoon, there was almost no correlation between LST and distance in Ahmedabad, with an R^2 of zero and a negative correlation of 0.07 in Surat. The evening and night exhibit a stronger negative correlation than morning for both cities. Ahmedabad in the evening and night during the summer had the strongest negative correlation among all diurnal periods, with R^2 of 0.61 and 0.62, respectively. For the winter months in Ahmedabad and Surat, there was a weak negative relationship in the afternoon with R^2 values of 0.07 and 0.06, respectively. During the evening and night, the negative correlations were strong for both cities.

Generally, Ahmedabad showed stronger correlations between LST, and distance compared to Surat, especially during the evening and night in both summer and winter. This indicates that Ahmedabad experienced a more pronounced surface UHI effect, with temperatures decreasing more rapidly with distance from the city center. Regarding diurnal variations, both cities exhibited the weakest correlation in the afternoon during both seasons, implying that the afternoon heat was more uniformly distributed across distances with not as much SUHI effect. In contrast, mornings, evenings, and nights showed stronger correlations, with temperatures decreasing as the distance increased, demonstrating that the surface UHI effect was more evident during the evening and night compared to the afternoon.

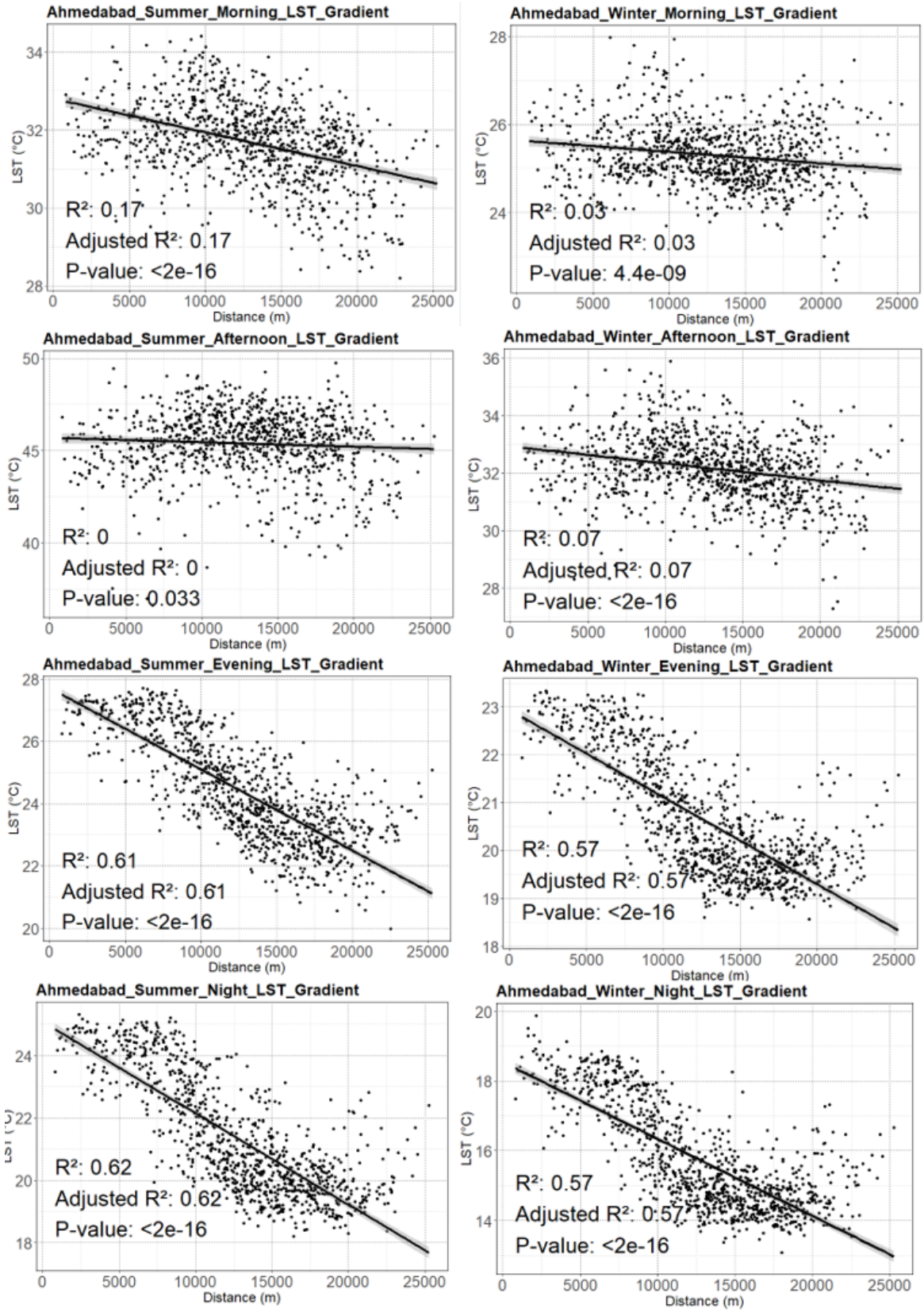


Figure 5.7: Ahmedabad LST gradient from the center of city towards rural areas during different times of the day and seasons.

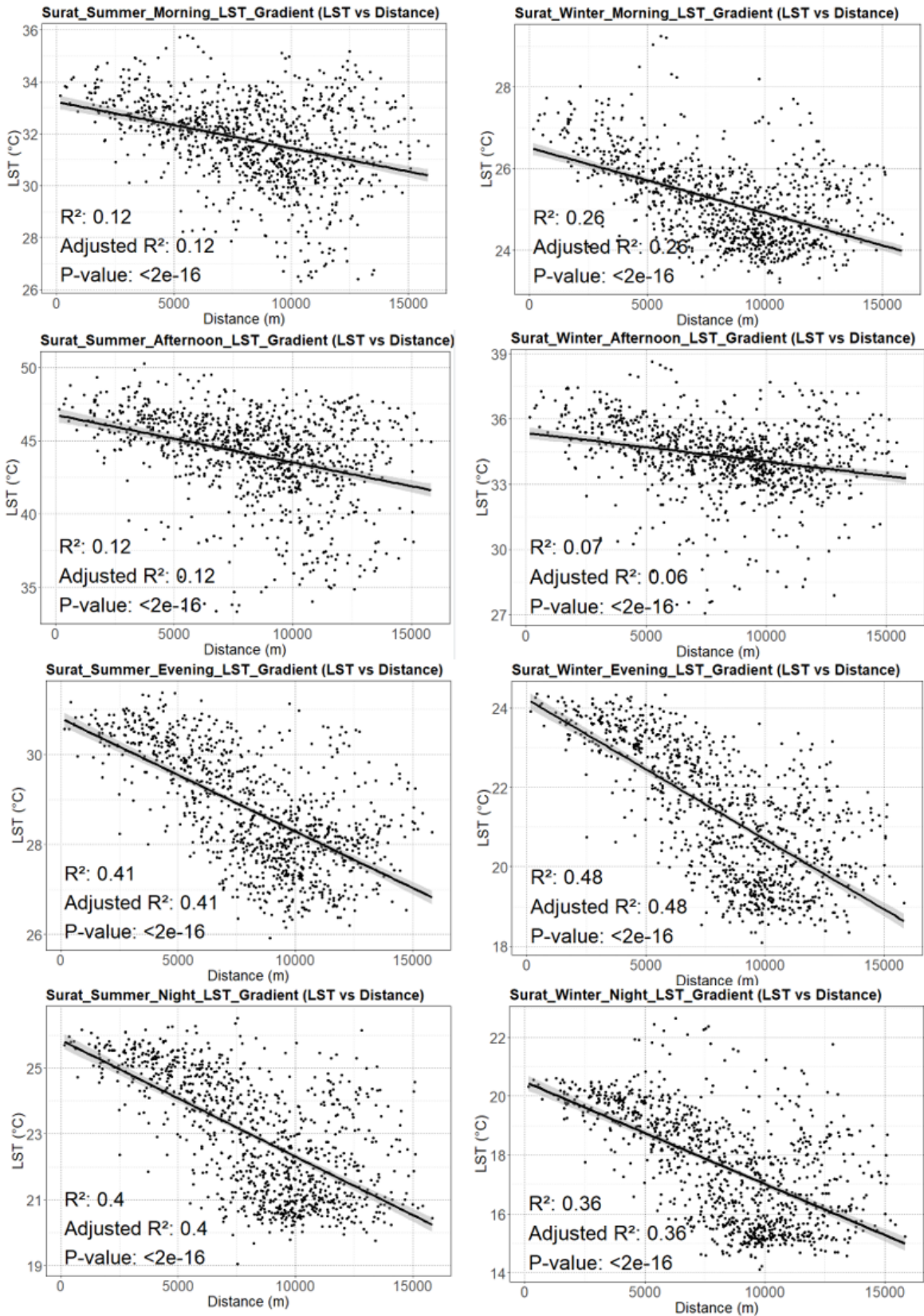


Figure 5.8: Surat LST gradient from the center of city towards rural areas during different times of the day and seasons

6. DISCUSSION AND CONCLUSION

In this study we analyzed the diurnal variations of the urban thermal characteristics over summer and winter in two cities (Ahmedabad and Surat) using the ECOSTRESS LST product and LCZs. We used a fusion strategy to obtain the urban LCZ delineations, which helped to better represent the vegetated classes and maintain the native resolution of 30m of Landsat. This study has shown that various urban types characterized by LCZ are closely related to LSTs and strongly affect the pattern of UHI. Specifically, compact midrise was consistently the highest, followed by large lowrise and compact lowrise areas during morning and afternoon. In contrast, LST over compact lowrise during evening and night was generally higher than large low rise. Open lowrise classes generally exhibit the lowest LSTs among the urban classes. Trees and Crops/Herbs classes consistently had the lowest LSTs across all diurnal periods and seasons.

Compact midrise areas were consistently hotter than compact lowrise because higher building volume and surface area and less vegetation in midrise zones lead to greater heat retention and reduced cooling from limited airflow. These taller buildings absorb and retain more heat during the day, releasing it slowly at night. Additionally, midrise buildings often use materials like concrete, brick, and tile, which have higher thermal inertia, storing and releasing more heat than those in lowrise areas (Stewart & Oke, 2012). The larger surface area exposed to solar radiation further enhances this effect. Also, compact midrise areas typically experience higher levels of human activity and energy use, such as air conditioning and vehicular traffic, contributing additional heat to the environment (Han et al., 2020). On the other hand, open lowrise areas were consistently the coolest as they usually have more green spaces and vegetation, which provide cooling through evapotranspiration, with trees and grass reducing the heat absorbed by buildings and pavements (Chang et al., 2021). Breaking the trend, compact lowrise were warmer in the evening and night, especially compared to large lowrise, because this type of zones often uses materials like concrete, brick and tiles forming dense urban fabric with tightly packed buildings that can retain a higher amount of incoming solar radiation. During the day, compact lowrise areas can absorb a significant amount of heat due to their dense urban fabric and limited green spaces. This heat is then released in the evening

and night, leading to higher temperatures relative to large lowrise areas, which might have more open spaces and vegetation, reducing overall heat absorption (Chang et al., 2021).

A similar study by Ferreira (Ferreira & Duarte, 2019) in the São Paulo metropolitan region aligns with our findings on LST distribution and its relationship with the LCZ scheme, utilizing similar methodologies with Aqua MODIS LST 8-day composite day and night data. While their study included eight LCZ urban classes and compared day and night temperatures, they also found that LSTs are not consistent across all urban classes. Specifically, they observed that the open high-rise class (LCZ-4, which was not present in our study area) exhibited marginally higher temperatures during the night. Another study by Chang (Chang et al., 2021) reported that temperature variations over different LCZs differed between day and night. They used ECOSTRESS data over a LCZ map and found that compact buildings were hotter during the day compared to open spaces buildings (open highrise, lowrise and midrise). They also found lowrise zones generally had higher LST than high rise zones in both compact and open urban structures however, our results were not directly comparable to these results as our study area consisted of only one tall building zone that was midrise (there were no highrise LCZs). Chang's results showed compact zones had higher nighttime LST than open zones, which is consistent with our findings.

Our study findings support and extend the understanding from previous research on how heterogeneous urban landforms affect LST distribution over urban landscapes. Specifically, our study focused on cities in developing countries, which largely lack compact, open, or large high-rise zones (Jedwab et al., 2021). This study analyzed the LCZ and LST relationship during various diurnal periods and established that the UHI effect is more prominent during the evening and night rather than in the morning and afternoon, when heat is more uniformly distributed, weakening the UHI effect (Spronken-Smith & Oke, 1998; Chapman et al., 2018). A significant temperature gradient can be observed in both cities during evening and night, with urban areas being 5 to 6 degrees hotter compared to their non-urban surroundings and this implies for both the seasons of summer and winter. This phenomenon is largely attributed to urban structures storing radiated energy during the day and releasing the stored heat at night (L. Zhao et al., 2014).

Inverse relationships between LST and distance from the city center were observed in the two study areas. We analyzed the temperature gradient from the city centroid towards the outskirts, where more vegetation typically exists. In general, more vegetation is associated with enhanced evapotranspiration, which can cool surfaces by converting solar radiation into latent heat rather than sensible heat (Mackey et al., 2012). Generally, the gradient showed no significant correlation between LST and distance in the afternoon. This is due to continued solar radiation heating the surface uniformly, thereby not creating a strong SUHI (Chang et al., 2022; G. Chen et al., 2023). In the morning, there was a moderate correlation between LST and distance. At this time, solar radiation is not as intense as in the afternoon due to the lower solar angle, and impervious surfaces are not as hot, leading to a moderate correlation (Allen et al., 2017; Lai et al., 2018). In contrast, there was a strong correlation between LST and distance during the evening and night. This is because, at the end of the day, urban structures release stored heat, keeping the city area warmer, while natural or vegetated areas cool down faster, thereby depicting a more pronounced SUHI (Chang et al., 2021; L. Zhao et al., 2014).

Based on visual inspection and manual interpretation of moderate resolution LST images, the study found that most of the hotspots during the summer season were located over multiple industrial areas classified as compact lowrise and large lowrise LCZs. It could be argued that actual residential classes might exhibit slightly lower overall LST if industrial zones were adequately classified in our classification map. A study by Carina (Portela et al., 2020) over São José dos Campos in the eastern portion of São Paulo State, Brazil also showed distinct hot spots over industrial and parking areas using Landsat data. Due to the alteration from natural landscapes to urban environments with heat-absorbing materials like asphalt and concrete, LST maps showed high temperatures in densely built industrial areas, where the combination of these materials and minimal vegetation creates the most extreme heat (Portela et al., 2020). Another case study by Lu (Y. Lu et al., 2021) in Wuhan, China using Landsat-8 showed the proportion of industrial areas has a significant impact on LST, even when the combined influences of land cover and building-group morphology are considered. This indicates that the anthropogenic heat generated by industrial activities is a major factor contributing to higher LSTs in industrial regions. Extensive use of combustion facilities like furnaces generates substantial waste heat discharged via chimneys, radiators, and cooling

water contributing to an increase in surrounding temperature. Additionally, industrial buildings often utilize metal panels with high short-wave radiation absorption compared to masonry materials commonly used elsewhere. This further amplifies heat retention within industrial zones (Y. Lu et al., 2021). Therefore, future studies in cities with a significant mixture of industrial areas within the city limits should carefully classify these zones to obtain an accurate picture of LST variations among residential urban settlements.

The findings of this study can be used by city planners and managers to help develop heat mitigation plans. Initially, the hotspots could be prioritized for heat mitigation strategies where temperatures reach 48 to 50°C in the summer afternoon. This could pose severe heat threats to the population living or working in these areas. Meanwhile effective methods should be implemented to reduce heat, one of which is increasing urban greenery through the planting of trees and the creation of green roofs and walls. Vegetation not only provides shade but also cools the air through the process of evapotranspiration (Mackey et al., 2012).

Another strategy involves the use of light-colored, highly reflective materials in urban infrastructures, such as rooftops, buildings, and roads. These materials have higher albedo, meaning they reflect more sunlight and absorb less heat. This reduces the amount of heat transferred into buildings, thus lowering indoor temperatures and reducing the need for air conditioning, which in turn decreases urban heat (Akbari & Matthews, 2012). Additionally, permeable pavements are an effective measure. Unlike traditional concrete and asphalt, permeable materials allow water to percolate through, which not only helps in reducing runoff but also aids in cooling the surface through evaporative cooling (Li et al., 2013).

Finally, public awareness and community involvement in implementing and maintaining green spaces, choosing reflective materials, and adopting energy-efficient practices are crucial. Education on the importance of reducing UHI and how individuals can contribute is essential for the long-term success of these strategies (Middel et al., 2020; Chang et al., 2021).

7. LIMITATIONS AND RECOMMENDATIONS

This research faced some limitations related to using ECOSTRESS and LCZ data. Even though ECOSTRESS has a repeat cycle within 3-5 days, the day and night LST data are not of the same day, causing inaccuracies and uncertainties. Additionally, the revisit cycles of ECOSTRESS sensor may lead to incomplete coverage of heatwave events, affecting the comprehensiveness of diurnal LST and SUHI research. ECOSTRESS data can also have missing grid cells due to cloud cover, further complicating the analysis. Additionally, it is influenced by view angle issues. The ECOSTRESS instrument captures data at varying angles due to the ISS's orbit where average view angle is considered to be $\sim \pm 26^\circ$ (Anderson et al., 2021). This variation in view angles can affect the accuracy and consistency of LST measurements, as different angles might capture different thermal emissions from the Earth's surface. Correction algorithms are applied to mitigate these effects, but some dependency on view angle variations remains.

Although this study demonstrated that ECOSTRESS data could characterize diurnal LST variations and spatial heterogeneity at four diurnal periods, a more extended period of ECOSTRESS observation is necessary to better interpret these variations. Future efforts should include image fusion using high temporal and spatial resolution data to enhance the comprehensiveness of diurnal LST and SUHI research. Image fusion techniques, such as those combining ECOSTRESS with data from other satellites like Landsat, MODIS, Sentinel-3 or GOES, can provide better temporal temperature measurements (Wu et al., 2015; G. Zhao et al., 2020; Chang et al., 2022). This approach can address the limitations posed by ECOSTRESS's 3–5-day revisit cycle and improve the accuracy and resolution of thermal data. Expanding the framework to include more cities with diverse landforms and climates will provide a more generalized understanding of urban thermal patterns. Moreover, further investigations are needed to refine the adjustment of ECOSTRESS LST data for diurnal cycle studies, which will help in better understanding diurnal SUHI patterns.

The LCZ data used in this research uses medium resolution remote sensing images like Landsat and Sentinel, with pixels resampled to a 100m resolution for classification. However, the accuracy of this LCZ remote-sensing mapping is low, with urban area mapping accuracy typically below 60% (Ma et al., 2021). This low classification accuracy is partly due to the

reliance on low resolution open-source data (EO input data table in Appendix 1), which does not provide detailed urban 3-D information relevant to LCZ types. Therefore, integrating 3-D urban form information is recommended to improve LCZ mapping accuracy by offering more detailed data.

LST data plays a crucial role in urban heat planning by assessing heat exposure and guiding mitigation strategies such as increasing green spaces and using heat-resistant materials to combat the UHI effect and reduce health risks. However, LST has limitations: it measures skin temperature and does not directly account for human heat stress, unlike indices like Heat Index or Wet Bulb Globe Temperature (WBGT), which consider factors like humidity and wind speed (D. Zhou et al., 2019). Variations in surface materials and vegetation can also affect LST accuracy. Therefore, while LST offers valuable insights for urban heat planning, integrating meteorological data and human heat stress indices is essential for a comprehensive understanding and effective mitigation tailored to urban conditions and population vulnerabilities, promoting resilient cities, and enhancing residents' well-being.

APPENDICES

Appendix 1. Earth observation (EO) input features for LCZ (Demuzere et al., 2021)

Sensor	Band / Ratio / Indicator
Landsat 8	<p>Median composites for B2 (red), B3 (green), B4 (red), B5 (Near infrared), B6/7 (Shortwave infrared 1/2), B10/11 (Thermal infrared 1/2)</p> <p>Median composites for BCI, NDBal, EBBI, NDWI, NDBI, NDVI</p> <p>10 and 90th percentile composites for NDVI</p>
Sentinel 1	<p>Single co-polarization (VV), dual-band cross-polarization (VH), and their ratio (VV/VH)</p> <p>Mean and standard deviation of VV and VH combined</p> <p>VH indicator</p>
Sentinel 2	<p>Median composite Red edge bands (B5, B6, B7)</p> <p>Median composite NDVI Red Edge 1 and 2</p> <p>Median composite S2REP, CSI, and SEI</p>
Other	<p>Global Forest Canopy Height (GFCH)</p> <p>DTM, DEM, DSM</p>

Appendix 2. Tables representing ECOSTRESS data download and processing statistics.

Numbers representing data available from downloads to various processing steps.

The average view angle of ECOSTRESS data is $\sim \pm 26^\circ$

	Total image downloaded 2018 to Mar-2024	Good Quality image after cloud and QC filtering	Visually selected quality images	Needed Geo-reference
Ahmedabad	550	209	161	23
Surat	522	198	149	29

Segregation of data availability for each season and time of day

	Summer	Winter
Ahmedabad	month 3,4,5,6	month 10,11,12,01,02
Morning_ 6 - 11:59	22	30
Afternoon_ 12 -17:59	21	35
Evening_ 18-23:59	8	18
Night_ 0 -5:59	7	20
	58	103
	Summer	Winter
Surat	month 3,4,5,6	month 10,11,12,01,02
Morning_ 6 - 11:59	21	28
Afternoon_ 12 -17:59	14	36
Evening_ 18-23:59	8	16
Night_ 0 -5:59	4	22
	47	102

Monthly data available after visually selecting and geo-referencing

Month	Ahmedabad	Surat
1	22	19
2	21	20
3	22	21
4	14	12
5	15	12
6	6	2
7	0	0
8	0	0
9	2	3
10	16	17
11	23	24
12	20	19
	161	149

Appendix 3. Ahmedabad LULC map accuracy and confusion matrix

For Ahmedabad		Validation data							
		Impervious	Soil	Forest	Crop/Herb	Water	Row_total	Producer's Acc	
RF Classified	Impervious	26	1	0	1	0	28	92.86%	
	Soil	1	6	0	6	0	13	46.15%	
	Forest	1	0	6	6	0	13	46.15%	
	Crop/Herb	0	2	1	45	0	48	93.75%	
	Water	0	0	0	0	9	9	100.00%	
	Col_total	28	9	7	58	9	111		
	User's Acc	92.86%	66.67%	85.71%	77.59%	100.00%		82.88%	Over_all Acc
		Kappa (k)		75%					

Appendix 4. Surat LULC map accuracy and confusion matrix

For Surat		Validation data							
		Impervious	Soil	Forest	Crop/ Herb	Water	Row_total	Producer's Acc	
RF Classified	Impervious	19	5	1	0	0	25	76.00%	
	Soil	1	3	0	0	0	4	75.00%	
	Forest	1	0	6	4	0	11	54.55%	
	Crop/ Herb	7	1	2	46	0	56	82.14%	
	Water	0	1	0	0	3	4	75.00%	
	Col_total	28	10	9	50	3	100		
	User's Acc	67.86%	30.00%	66.67%	92.00%	100.00%		77.00%	Over_all Acc
		Kappa (k)	64%						

Appendix 5. Ahmedabad Landsat-8 scenes used for LULC classification in Google Earth Engine.

LANDSAT/LC08/C02/T1_L2/LC08_148044_20200123
 LANDSAT/LC08/C02/T1_L2/LC08_148044_20200208
 LANDSAT/LC08/C02/T1_L2/LC08_148044_20200224
 LANDSAT/LC08/C02/T1_L2/LC08_148044_20200412
 LANDSAT/LC08/C02/T1_L2/LC08_148044_20200428
 LANDSAT/LC08/C02/T1_L2/LC08_148044_20200514
 LANDSAT/LC08/C02/T1_L2/LC08_148044_20201005
 LANDSAT/LC08/C02/T1_L2/LC08_148044_20201021
 LANDSAT/LC08/C02/T1_L2/LC08_148044_20201122
 LANDSAT/LC08/C02/T1_L2/LC08_148044_20201208
 LANDSAT/LC08/C02/T1_L2/LC08_148044_20201224
 LANDSAT/LC08/C02/T1_L2/LC08_149044_20200114
 LANDSAT/LC08/C02/T1_L2/LC08_149044_20200130
 LANDSAT/LC08/C02/T1_L2/LC08_149044_20200302
 LANDSAT/LC08/C02/T1_L2/LC08_149044_20200318
 LANDSAT/LC08/C02/T1_L2/LC08_149044_20200403
 LANDSAT/LC08/C02/T1_L2/LC08_149044_20200419
 LANDSAT/LC08/C02/T1_L2/LC08_149044_20200505
 LANDSAT/LC08/C02/T1_L2/LC08_149044_20200521
 LANDSAT/LC08/C02/T1_L2/LC08_149044_20201012
 LANDSAT/LC08/C02/T1_L2/LC08_149044_20201028
 LANDSAT/LC08/C02/T1_L2/LC08_149044_20201129
 LANDSAT/LC08/C02/T1_L2/LC08_149044_20201215

Appendix 6. Surat Landsat-8 scenes used for LULC classification in Google earth Engine.

LANDSAT/LC08/C02/T1_L2/LC08_148045_20200123
LANDSAT/LC08/C02/T1_L2/LC08_148045_20200208
LANDSAT/LC08/C02/T1_L2/LC08_148045_20200224
LANDSAT/LC08/C02/T1_L2/LC08_148045_20200428
LANDSAT/LC08/C02/T1_L2/LC08_148045_20200514
LANDSAT/LC08/C02/T1_L2/LC08_148045_20201122
LANDSAT/LC08/C02/T1_L2/LC08_148045_20201224
LANDSAT/LC08/C02/T1_L2/LC08_148046_20200123
LANDSAT/LC08/C02/T1_L2/LC08_148046_20200208
LANDSAT/LC08/C02/T1_L2/LC08_148046_20200224
LANDSAT/LC08/C02/T1_L2/LC08_148046_20200412
LANDSAT/LC08/C02/T1_L2/LC08_148046_20200428
LANDSAT/LC08/C02/T1_L2/LC08_148046_20200514
LANDSAT/LC08/C02/T1_L2/LC08_148046_20201122
LANDSAT/LC08/C02/T1_L2/LC08_148046_20201224

List of References

- Akbari, H., & Matthews, H. D. (2012). Global cooling updates: Reflective roofs and pavements. *Energy and Buildings*, 55, 2–6. <https://doi.org/10.1016/j.enbuild.2012.02.055>
- Allen, M., Voogt, J., & Christen, A. (2017). Time-Continuous Hemispherical Urban Surface Temperatures. *Remote Sensing*, 10(1), 3. <https://doi.org/10.3390/rs10010003>
- Anderson, M. C., Yang, Y., Xue, J., Knipper, K. R., Yang, Y., Gao, F., Hain, C. R., Kustas, W. P., Cawse-Nicholson, K., Hulley, G., Fisher, J. B., Alfieri, J. G., Meyers, T. P., Prueger, J., Baldocchi, D. D., & Rey-Sanchez, C. (2021). Interoperability of ECOSTRESS and Landsat for mapping evapotranspiration time series at sub-field scales. *Remote Sensing of Environment*, 252, 112189. <https://doi.org/10.1016/j.rse.2020.112189>
- AR5 Climate Change 2014: Mitigation of Climate Change — IPCC. (n.d.). Retrieved June 10, 2024, from <https://www.ipcc.ch/report/ar5/wg3/>
- Argüeso, D., Evans, J. P., Pitman, A. J., & Di Luca, A. (2015). Effects of City Expansion on Heat Stress under Climate Change Conditions. *PLOS ONE*, 10(2), e0117066. <https://doi.org/10.1371/journal.pone.0117066>
- Bechtel, B., Alexander, P. J., Böhner, J., Ching, J., Conrad, O., Feddema, J., Mills, G., See, L., & Stewart, I. (2015). Mapping Local Climate Zones for a Worldwide Database of the Form and Function of Cities. *ISPRS International Journal of Geo-Information*, 4(1), 199–219. <https://doi.org/10.3390/ijgi4010199>
- Bokaie, M., Zarkesh, M. K., Arasteh, P. D., & Hosseini, A. (2016). Assessment of Urban Heat Island based on the relationship between land surface temperature and Land Use/ Land Cover in Tehran. *Sustainable Cities and Society*, 23, 94–104. <https://doi.org/10.1016/j.scs.2016.03.009>
- Chang, Y., Xiao, J., Li, X., Middel, A., Zhang, Y., Gu, Z., Wu, Y., & He, S. (2021). Exploring diurnal thermal variations in urban local climate zones with ECOSTRESS land surface temperature data. *Remote Sensing of Environment*, 263, 112544. <https://doi.org/10.1016/j.rse.2021.112544>
- Chang, Y., Xiao, J., Li, X., Zhou, D., & Wu, Y. (2022). Combining GOES-R and ECOSTRESS land surface temperature data to investigate diurnal variations of surface urban heat island. *Science of The Total Environment*, 823, 153652. <https://doi.org/10.1016/j.scitotenv.2022.153652>
- Chapman, S., Thatcher, M., Salazar, A., Watson, J. E. M., & McAlpine, C. A. (2018). The Effect of Urban Density and Vegetation Cover on the Heat Island of a Subtropical City. *Journal of Applied Meteorology and Climatology*, 57(11), 2531–2550. <https://doi.org/10.1175/JAMC-D-17-0316.1>
- Chen, G., Chen, Y., Tan, X., Zhao, L., Cai, Y., & Li, L. (2023). Assessing the urban heat island effect of different local climate zones in Guangzhou, China. *Building and Environment*, 244, 110770. <https://doi.org/10.1016/j.buildenv.2023.110770>
- Chen, Y.-C., Chiu, H.-W., Su, Y.-F., Wu, Y.-C., & Cheng, K.-S. (2017). Does urbanization increase diurnal land surface temperature variation? Evidence and implications.

- Landscape and Urban Planning*, 157, 247–258.
<https://doi.org/10.1016/j.landurbplan.2016.06.014>
- Clinton, N., & Gong, P. (2013). MODIS detected surface urban heat islands and sinks: Global locations and controls. *Remote Sensing of Environment*, 134, 294–304.
<https://doi.org/10.1016/j.rse.2013.03.008>
- Danylo, O., See, L., Bechtel, B., Schepaschenko, D., & Fritz, S. (2016). Contributing to WUDAPT: A Local Climate Zone Classification of Two Cities in Ukraine. *IEEE Journal of Selected Topics in Applied Earth Observations and Remote Sensing*, 9(5), 1841–1853.
<https://doi.org/10.1109/JSTARS.2016.2539977>
- Deilami, K., Kamruzzaman, Md., & Liu, Y. (2018). Urban heat island effect: A systematic review of spatio-temporal factors, data, methods, and mitigation measures. *International Journal of Applied Earth Observation and Geoinformation*, 67, 30–42.
<https://doi.org/10.1016/j.jag.2017.12.009>
- Demuzere, M., Kittner, J., & Bechtel, B. (2021). LCZ Generator: A Web Application to Create Local Climate Zone Maps. *Frontiers in Environmental Science*, 9.
<https://doi.org/10.3389/fenvs.2021.637455>
- Demuzere, M., Kittner, J., Martilli, A., Mills, G., Moede, C., Stewart, I. D., van Vliet, J., & Bechtel, B. (2022). A global map of local climate zones to support earth system modelling and urban-scale environmental science. *Earth System Science Data*, 14(8), 3835–3873. <https://doi.org/10.5194/essd-14-3835-2022>
- Feng, X., & Myint, S. (2016). Exploring the effect of neighboring land cover pattern on land surface temperature of central building objects. *Building and Environment*, 95, 346–354.
<https://doi.org/10.1016/j.buildenv.2015.09.019>
- Ferreira, L. S., & Duarte, D. H. S. (2019). Exploring the relationship between urban form, land surface temperature and vegetation indices in a subtropical megacity. *Urban Climate*, 27, 105–123. <https://doi.org/10.1016/j.uclim.2018.11.002>
- Firozjaei, M. K., Kiavarz, M., Alavipanah, S. K., Lakes, T., & Qureshi, S. (2018). Monitoring and forecasting heat island intensity through multi-temporal image analysis and cellular automata-Markov chain modelling: A case of Babol city, Iran. *Ecological Indicators*, 91, 155–170. <https://doi.org/10.1016/j.ecolind.2018.03.052>
- Gohain, K. J., Mohammad, P., & Goswami, A. (2021). Assessing the impact of land use land cover changes on land surface temperature over Pune city, India. *Quaternary International*, 575–576, 259–269. <https://doi.org/10.1016/j.quaint.2020.04.052>
- Guha, S., Govil, H., Dey, A., & Gill, N. (2018). Analytical study of land surface temperature with NDVI and NDBI using Landsat 8 OLI and TIRS data in Florence and Naples city, Italy. *European Journal of Remote Sensing*, 51(1), 667–678.
<https://doi.org/10.1080/22797254.2018.1474494>
- Han, J., Liu, J., Liu, L., & Ye, Y. (2020). Spatiotemporal Changes in the Urban Heat Island Intensity of Distinct Local Climate Zones: Case Study of Zhongshan District, Dalian, China. *Complexity*, 2020, e8820338. <https://doi.org/10.1155/2020/8820338>

- Hook, S. J., Cawse-Nicholson, K., Barsi, J., Radocinski, R., Hulley, G. C., Johnson, W. R., Rivera, G., & Markham, B. (2020). In-Flight Validation of the ECOSTRESS, Landsats 7 and 8 Thermal Infrared Spectral Channels Using the Lake Tahoe CA/NV and Salton Sea CA Automated Validation Sites. *IEEE Transactions on Geoscience and Remote Sensing*, *58*(2), 1294–1302. <https://doi.org/10.1109/TGRS.2019.2945701>
- Hulley, G., Gottsche, F. M., Rivera, G., Hook, S. J., Freepartner, R. J., Martin, M. A., Cawse-Nicholson, K., & Johnson, W. R. (2022). Validation and Quality Assessment of the ECOSTRESS Level-2 Land Surface Temperature and Emissivity Product. *IEEE Transactions on Geoscience and Remote Sensing*, *60*, 1–23. <https://doi.org/10.1109/TGRS.2021.3079879>
- Hulley, G., Shivers, S., Wetherley, E., & Cudd, R. (2019). New ECOSTRESS and MODIS Land Surface Temperature Data Reveal Fine-Scale Heat Vulnerability in Cities: A Case Study for Los Angeles County, California. *Remote Sensing*, *11*(18), 2136. <https://doi.org/10.3390/rs11182136>
- Jedwab, R., Loungani, P., & Yezer, A. (2021). Comparing cities in developed and developing countries: Population, land area, building height and crowding. *Regional Science and Urban Economics*, *86*, 103609. <https://doi.org/10.1016/j.regsciurbeco.2020.103609>
- Kustas, W., & Anderson, M. (2009). Advances in thermal infrared remote sensing for land surface modeling. *Agricultural and Forest Meteorology*, *149*(12), 2071–2081. <https://doi.org/10.1016/j.agrformet.2009.05.016>
- Lai, J., Zhan, W., Huang, F., Voogt, J., Bechtel, B., Allen, M., Peng, S., Hong, F., Liu, Y., & Du, P. (2018). Identification of typical diurnal patterns for clear-sky climatology of surface urban heat islands. *Remote Sensing of Environment*, *217*, 203–220. <https://doi.org/10.1016/j.rse.2018.08.021>
- Leconte, F., Bouyer, J., Claverie, R., & Pétrissans, M. (2015). Using Local Climate Zone scheme for UHI assessment: Evaluation of the method using mobile measurements. *Building and Environment*, *83*, 39–49. <https://doi.org/10.1016/j.buildenv.2014.05.005>
- Li, H., Harvey, J. T., Holland, T. J., & Kayhanian, M. (2013). The use of reflective and permeable pavements as a potential practice for heat island mitigation and stormwater management. *Environmental Research Letters*, *8*(1), 015023. <https://doi.org/10.1088/1748-9326/8/1/015023>
- Lu, L., Weng, Q., Xiao, D., Guo, H., Li, Q., & Hui, W. (2020). Spatiotemporal Variation of Surface Urban Heat Islands in Relation to Land Cover Composition and Configuration: A Multi-Scale Case Study of Xi'an, China. *Remote Sensing*, *12*(17), 2713. <https://doi.org/10.3390/rs12172713>
- Lu, Y., Yue, W., & Huang, Y. (2021). Effects of Land Use on Land Surface Temperature: A Case Study of Wuhan, China. *International Journal of Environmental Research and Public Health*, *18*(19), 9987. <https://doi.org/10.3390/ijerph18199987>

- Ma, L., Zhu, X., Qiu, C., Blaschke, T., & Li, M. (2021). Advances of Local Climate Zone Mapping and Its Practice Using Object-Based Image Analysis. *Atmosphere*, *12*(9), 1146. <https://doi.org/10.3390/atmos12091146>
- Mackey, C. W., Lee, X., & Smith, R. B. (2012). Remotely sensing the cooling effects of city scale efforts to reduce urban heat island. *Building and Environment*, *49*, 348–358. <https://doi.org/10.1016/j.buildenv.2011.08.004>
- Malik, S., Pal, S. C., Sattar, A., Singh, S. K., Das, B., Chakraborty, R., & Mohammad, P. (2020). Trend of extreme rainfall events using suitable Global Circulation Model to combat the water logging condition in Kolkata Metropolitan Area. *Urban Climate*, *32*, 100599. <https://doi.org/10.1016/j.uclim.2020.100599>
- Middel, A., Hüb, K., Brazel, A. J., Martin, C. A., & Guhathakurta, S. (2014). Impact of urban form and design on mid-afternoon microclimate in Phoenix Local Climate Zones. *Landscape and Urban Planning*, *122*, 16–28. <https://doi.org/10.1016/j.landurbplan.2013.11.004>
- Middel, A., Turner, V. K., Schneider, F. A., Zhang, Y., & Stiller, M. (2020). Solar reflective pavements—A policy panacea to heat mitigation? *Environmental Research Letters*, *15*(6), 064016. <https://doi.org/10.1088/1748-9326/ab87d4>
- Nichol, J. E. (1994). A GIS-based approach to microclimate monitoring in Singapore's high-rise housing estates. *Photogrammetric Engineering & Remote Sensing*, *60*(10), 1225–1232.
- Oke, T. R. (1982). The energetic basis of the urban heat island. *Quarterly Journal of the Royal Meteorological Society*, *108*(455), 1–24. <https://doi.org/10.1002/qj.49710845502>
- Peel, M. C., Finlayson, B. L., & McMahon, T. A. (2007). Updated world map of the Köppen-Geiger climate classification. *Hydrology and Earth System Sciences*, *11*(5), 1633–1644. <https://doi.org/10.5194/hess-11-1633-2007>
- Peres, L. D. F., Lucena, A. J. D., Rotunno Filho, O. C., & França, J. R. D. A. (2018). The urban heat island in Rio de Janeiro, Brazil, in the last 30 years using remote sensing data. *International Journal of Applied Earth Observation and Geoinformation*, *64*, 104–116. <https://doi.org/10.1016/j.jag.2017.08.012>
- Portela, C. I., Massi, K. G., Rodrigues, T., & Alcântara, E. (2020). Impact of urban and industrial features on land surface temperature: Evidences from satellite thermal indices. *Sustainable Cities and Society*, *56*, 102100. <https://doi.org/10.1016/j.scs.2020.102100>
- Rizwan, A. M., Dennis, L. Y. C., & Liu, C. (2008). A review on the generation, determination and mitigation of Urban Heat Island. *Journal of Environmental Sciences*, *20*(1), 120–128. [https://doi.org/10.1016/S1001-0742\(08\)60019-4](https://doi.org/10.1016/S1001-0742(08)60019-4)
- Shahfahad, Naikoo, M. W., Towfiqul Islam, A. R. Md., Mallick, J., & Rahman, A. (2022). Land use/land cover change and its impact on surface urban heat island and urban thermal comfort in a metropolitan city. *Urban Climate*, *41*, 101052. <https://doi.org/10.1016/j.uclim.2021.101052>
- Shahfahad, Rihan, M., Naikoo, M. W., Ali, M. A., Usmani, T. M., & Rahman, A. (2021). Urban Heat Island Dynamics in Response to Land-Use/Land-Cover Change in the Coastal City

- of Mumbai. *Journal of the Indian Society of Remote Sensing*, 49(9), 2227–2247.
<https://doi.org/10.1007/s12524-021-01394-7>
- Siddiqui, A., Kushwaha, G., Nikam, B., Srivastav, S. K., Shelar, A., & Kumar, P. (2021). Analysing the day/night seasonal and annual changes and trends in land surface temperature and surface urban heat island intensity (SUHII) for Indian cities. *Sustainable Cities and Society*, 75, 103374. <https://doi.org/10.1016/j.scs.2021.103374>
- Simanjuntak, R. M., Kuffer, M., & Reckien, D. (2019). Object-based image analysis to map local climate zones: The case of Bandung, Indonesia. *Applied Geography*, 106, 108–121.
<https://doi.org/10.1016/j.apgeog.2019.04.001>
- Spronken-Smith, R. A., & Oke, T. R. (1998). The thermal regime of urban parks in two cities with different summer climates. *International Journal of Remote Sensing*, 19(11), 2085–2104. <https://doi.org/10.1080/014311698214884>
- Stewart, I. D., & Oke, T. R. (2012). Local Climate Zones for Urban Temperature Studies. *Bulletin of the American Meteorological Society*, 93(12), 1879–1900.
<https://doi.org/10.1175/BAMS-D-11-00019.1>
- Středová, H., Chuchma, F., Rožnovský, J., & Středa, T. (2021). Local Climate Zones, Land Surface Temperature and Air Temperature Interactions: Case Study of Hradec Králové, the Czech Republic. *ISPRS International Journal of Geo-Information*, 10(10), 704.
<https://doi.org/10.3390/ijgi10100704>
- Sun, C., Sun, C., Yang, Z., Zhang, J., & Deng, Y. (2016). Urban Land Development for Industrial and Commercial Use: A Case Study of Beijing. *Sustainability*, 8(12), 1323.
<https://doi.org/10.3390/su8121323>
- UN, H. (2016). *Urbanization and development: Emerging futures*. UN-Habitat.
- UN-Habitat. (2011). *Human Development Report 2011*. United Nations.
<https://hdr.undp.org/content/human-development-report-2011>
- United Nations. (2019). *World urbanization prospects: The 2018 revision*. United Nations.
- US EPA, O. (2014). *Heat Island Compendium*. <https://www.epa.gov/heatislands/heat-island-compendium>
- Voogt, J. A., & Oke, T. R. (2003). Thermal remote sensing of urban climates. *Remote Sensing of Environment*, 86(3), 370–384. [https://doi.org/10.1016/S0034-4257\(03\)00079-8](https://doi.org/10.1016/S0034-4257(03)00079-8)
- Wei, L., & Sobrino, J. A. (2024). Surface urban heat island analysis based on local climate zones using ECOSTRESS and Landsat data: A case study of Valencia city (Spain). *International Journal of Applied Earth Observation and Geoinformation*, 130, 103875.
<https://doi.org/10.1016/j.jag.2024.103875>
- Weng, Q., Firozjaei, M. K., Sedighi, A., Kiavarz, M., & Alavipanah, S. K. (2019). Statistical analysis of surface urban heat island intensity variations: A case study of Babol city, Iran. *GIScience & Remote Sensing*, 56(4), 576–604.
<https://doi.org/10.1080/15481603.2018.1548080>
- Wu, M., Wu, C., Huang, W., Niu, Z., Wang, C., Li, W., & Hao, P. (2015). An improved high spatial and temporal data fusion approach for combining Landsat and MODIS data to

- generate daily synthetic Landsat imagery. *Information Fusion*, 31. <https://doi.org/10.1016/j.inffus.2015.12.005>
- Yang, J., Zhan, Y., Xiao, X., Xia, J. C., Sun, W., & Li, X. (2020). Investigating the diversity of land surface temperature characteristics in different scale cities based on local climate zones. *Urban Climate*, 34, 100700. <https://doi.org/10.1016/j.uclim.2020.100700>
- Yow, D. M. (2007). Urban Heat Islands: Observations, Impacts, and Adaptation. *Geography Compass*, 1(6), 1227–1251. <https://doi.org/10.1111/j.1749-8198.2007.00063.x>
- Zhang, W., Huang, Y., Yu, Y., & Sun, W. (2011). Empirical models for estimating daily maximum, minimum and mean air temperatures with MODIS land surface temperatures. *International Journal of Remote Sensing*, 32(24), 9415–9440. <https://doi.org/10.1080/01431161.2011.560622>
- Zhang, X., Zhong, T., Feng, X., & Wang, K. (2009). Estimation of the relationship between vegetation patches and urban land surface temperature with remote sensing. *International Journal of Remote Sensing*, 30(8), 2105–2118. <https://doi.org/10.1080/01431160802549252>
- Zhao, G., Zhang, Y., Tan, J., Li, C., & Ren, Y. (2020). A Data Fusion Modeling Framework for Retrieval of Land Surface Temperature from Landsat-8 and MODIS Data. *Sensors*, 20(15), 4337. <https://doi.org/10.3390/s20154337>
- Zhao, L., Lee, X., Smith, R. B., & Oleson, K. (2014). Strong contributions of local background climate to urban heat islands. *Nature*, 511(7508), 216–219. <https://doi.org/10.1038/nature13462>
- Zhao, Z., Sharifi, A., Dong, X., Shen, L., & He, B.-J. (2021). Spatial Variability and Temporal Heterogeneity of Surface Urban Heat Island Patterns and the Suitability of Local Climate Zones for Land Surface Temperature Characterization. *Remote Sensing*, 13(21), 4338. <https://doi.org/10.3390/rs13214338>
- Zhou, D., Xiao, J., Bonafoni, S., Berger, C., Deilami, K., Zhou, Y., Froking, S., Yao, R., Qiao, Z., & Sobrino, J. A. (2019). Satellite Remote Sensing of Surface Urban Heat Islands: Progress, Challenges, and Perspectives. *Remote Sensing*, 11(1), 48. <https://doi.org/10.3390/rs11010048>
- Zhou, W., Huang, G., & Cadenasso, M. L. (2011). Does spatial configuration matter? Understanding the effects of land cover pattern on land surface temperature in urban landscapes. *Landscape and Urban Planning*, 102(1), 54–63. <https://doi.org/10.1016/j.landurbplan.2011.03.009>
- Zhou, X., Okaze, T., Ren, C., Cai, M., Ishida, Y., Watanabe, H., & Mochida, A. (2020). Evaluation of urban heat islands using local climate zones and the influence of sea-land breeze. *Sustainable Cities and Society*, 55, 102060. <https://doi.org/10.1016/j.scs.2020.102060>
- Zölch, T., Maderspacher, J., Wamsler, C., & Pauleit, S. (2016). Using green infrastructure for urban climate-proofing: An evaluation of heat mitigation measures at the micro-scale.

Urban Forestry & Urban Greening, 20, 305–316.
<https://doi.org/10.1016/j.ufug.2016.09.011>